WILEY

Advanced ESR Methods in Polymer Research

Edited by **Shulamith Schlick**

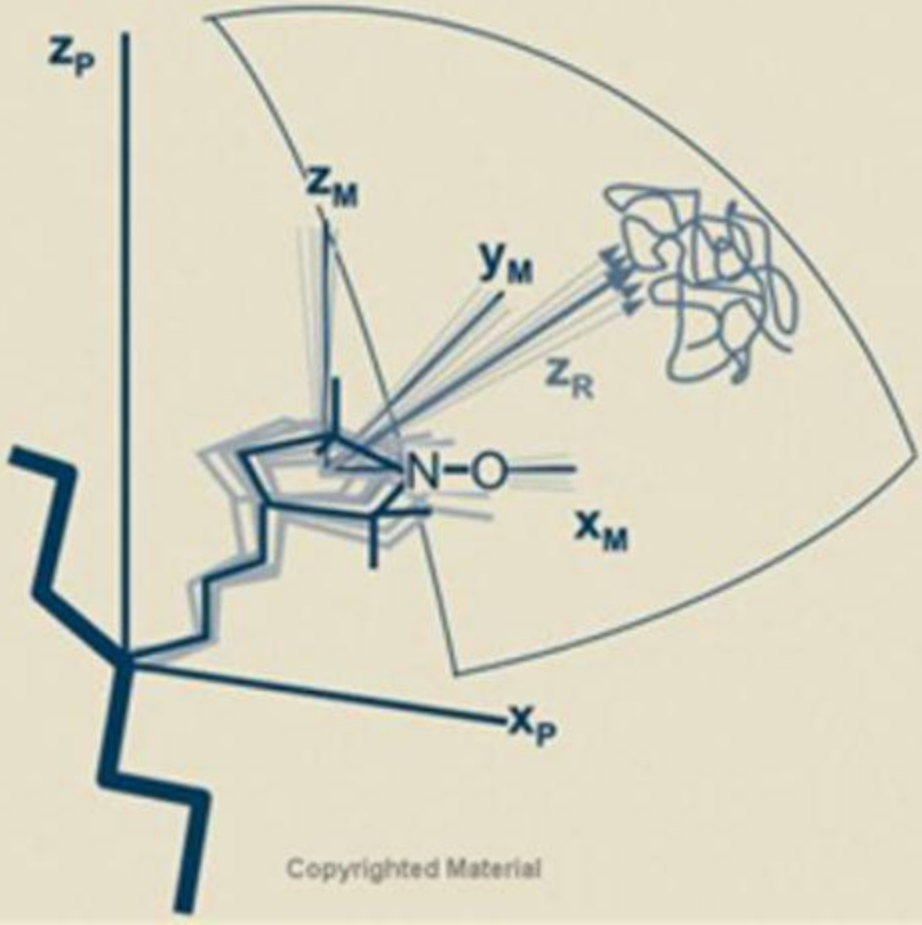

ADVANCED ESR METHODS IN POLYMER RESEARCH

Edited by

SHULAMITH SCHLICK
University of Detroit Mercy
Detroit, Michigan

WILEY-INTERSCIENCE
A John Wiley & Sons, Inc., Publication

Published by John Wiley & Sons, Inc., Hoboken, New Jersey
Published simultaneously in Canada

Library of Congress Cataloging-in-Publication Data:

Advanced ESR methods in polymer research/edited by Shulamith Schlick.
p.cm.
Includes bibliographical references and index.
ISBN-13: 978-0-471-73189-4
ISBN-10: 0-471-73189-7
1. Electron paramagnetic resonance—Research. 2. Polymers—Research. I. Schlick, Shulamith.

QC763.A32.2006
547'.7046—dc22

2006044267

Printed in the United States of America
10 9 8 7 6 5 4 3 2 1

CONTENTS

PREFACE

In May 1994, I visited Professor Bengt Rånby at the Royal Institute of Technology in Stockholm, Sweden. Professor Rånby, at that time Emeritus, was enthusiastic about his numerous projects, including collaborations with Chinese scientists. On that occasion, I mentioned to him how useful his 1977 book entitled *ESR Spectroscopy in Polymer Research*, which he wrote together with J.F. Rabek, had been to me and many of my colleagues over the years. Professor Rånby confided that he planned a sequel, which "would be published sometime soon." I was hopeful, and expectant, but this was not to be.

So, what to do with all the excitement in the electron spin resonance (ESR) community over the extraordinary advances in ESR techniques in the last 20 years, techniques that have been used in Polymer Science? The pulsed, high field, double resonance, and DEER experiments, ESR imaging, simulations? Someone must tell the story, and I took the challenge.

In the winter of 2004, I was on sabbatical at the Max Planck Institute for Polymer Research in Mainz, Germany, shared an office with Gunnar Jeschke, and worked with him on the ESR chapter for the *Encyclopedia of Polymer Science and Technology (EPST)*.* Jacqueline I. Kroschwitz, the editor of *EPST*, encouraged me to enlarge the chapter into a full volume. In all planning and writing stages, I benefited greatly from numerous discussions with Gunnar, who has enriched the book by the three chapters that he contributed.

The final content of this book evolved during many talks with students and coworkers at UDM and colleagues at other institutions, and during long walks in my neighborhood. It took the talent, dedication, and patience of the contributors to travel

* Schlick, S.; Jeschke, G. Electron Spin Resonance, In *Encyclopedia of Polymer Science and Engineering*, Kroschwitz, J.I., Ed.; Wiley-Interscience: New York, NY, 2004; Chap. 9, pp. 614–651 (web and hardcopy editions).

through the seemingly endless revisions and to arrive at the published volume. I am grateful to Arza Seidel and her team at Wiley for guidance during all stages of this project.

Part I of the present volume includes the fundamentals and developments of the ESR experimental and simulations techniques. This part could be a valuable introduction to students interested in ESR, or in the ESR of polymers. Part II describes the wide range of applications to polymeric systems, from living radical polymerization to block copolymers, polymer solutions, ion-containing polymers, polymer lattices, membranes in fuel cells, degradation, polymer coatings, dendrimers, and conductive polymers: a world of ESR cum polymers. It is my hope that the wide range of ESR techniques and applications will be of interest to students and mature polymer scientists and will encourage them to apply ESR methods more widely to polymeric materials. And I extend an invitation to ESR specialists, to apply their talents to polymers.

SHULAMITH SCHLICK

February 2006

CONTRIBUTORS

David R. Bauer, Research and Advanced Engineering, Ford Motor Company, Dearborn, Michigan, *ESR Studies of Photooxidation and Stabilization of Polymer Coatings (Chapter 10).*

David E. Budil, Department of Chemistry, Northeastern University, Boston, Massachusetts, *Calculating Slow-Motion ESR Spectra of Spin-Labeled Polymers (Chapter 3).*

Keith A. Earle, Department of Physics, University of Albany (SUNY), Albany, New York, *Calculating Slow-Motion ESR Spectra of Spin-Labeled Polymers (Chapter 3).*

John L. Gerlock, Ford Motor Company (retired), *ESR Studies of Photooxidation and Stabilization of Polymer Coatings (Chapter 10).*

Gunnar Jeschke, MPI for Polymer Research, Mainz, Germany, *Continuous-Wave and Pulsed ESR Methods (Chapter 1), Double Resonance ESR Methods (Chapter 2), Site-Specific Information on Macromolecular Materials by Combining CW and Pulsed ESR on Spin Probes (Chapter 7).*

Astushi Kajiwara, Nara University of Education, Nara, Japan, *ESR Study of Radicals in Conventional Radical Polymerization Using Radical Precursors Prepared by Atom Transfer Radical Polymerization (Chapter 5).*

Victor I. Krinichnyi, Institute of Problems of Chemical Physics, Chernogolovka, Moscow Region, Russia, *High-Field ESR Spectroscopy of Conductive Polymers (Chapter 12).*

Krzysztof Kruczala, Faculty of Chemistry, Jagiellonian University, Cracow, Poland, *Spatially Resolved Degradation in Heterophasic Polymers From 1D and 2D Spectral-Spatial ESR Imaging Experiments (Chapter 9)* .

Krzysztof Matyjaszewski, Department of Chemistry, Carnegie Mellon University, Pittsburgh, Pennsylvania, *ESR Study of Radicals in Conventional Radical Polymerization Using Radical Precursors Prepared by Atom Transfer Radical Polymerization (Chapter 5).*

M. Francesca Ottaviani, Institute of Chemical Sciences, University of Urbino, Urbino, Italy, *Characterization of Dendrimer Structures by ESR Techniques (Chapter 11).*

Jan Pilar, Institute of Macromolecular Chemistry, Academy of Sciences of the Czech Republic, Prague, Czech Republic, *Local Dynamics of Polymers in Solution by Spin-Label ESR (Chapter 6).*

Emil Roduner, Institute of Physical Chemistry, University of Stuttgart, Stuttgart, Germany, *ESR Methods for Assessing the Stability of Polymer Membranes Used in Fuel Cells (Chapter 8).*

Shulamith Schlick, Department of Chemistry and Biochemistry, University of Detroit Mercy, Detroit, Michigan, *Continuous-Wave and Pulsed ESR Methods (Chapter 1)*, *ESR Imaging (Chapter 4)*, *ESR Methods for Assessing the Stability of Polymer Membranes Used in Fuel Cells (Chapter 8)*, *Spatially Resolved Degradation in Heterophasic Polymers From 1D and 2D Spectral-Spatial ESR Imaging Experiments (Chapter 9).*

Nicholas J. Turro, Department of Chemistry, Columbia University, New York, *Characterization of Dendrimer Structures by ESR Techniques (Chapter 11).*

12*

HIGH-FIELD ESR SPECTROSCOPY OF CONDUCTIVE POLYMERS

VICTOR I. KRINICHNYI
Institute of Problems of Chemical Physics, Chernogolovka, Russia

Contents

1. INTRODUCTION

Various low-dimensional compounds can be considered as organic conductors; organic conductive polymers are of special interest,[1,2] due to their potential applications in molecular electronics. A major scientific goal is to reinforce the human brain with the ability of a computer. However, a convenient computer is based on three-dimensional (3D) silicon technology, whereas human organisms consist of low-dimensional biological

* This chapter is dedicated to my wife, Tatiana Krinichnaya.

Advanced ESR Methods in Polymer Research, edited by Shulamith Schlick.

systems. So, the future computer based on organic conductive polymers, combined with biosystems, is expected to increase considerably the power of human comprehension.

Initially, π-conjugated polymers are insulators. Their conductivity can be controlled by the chemical–electrochemical introduction of dopants, for example, acids or metal ions, which accept from a chain or inject to a chain an elemental charge. Consequently, the conductivity of a polymer increases up to $\approx 10^{-5}$–1 S cm^{-1} (semiconductor) or even up to $\approx 10^{2}$–10^{6} S cm^{-1} (metal).[1]

Polyacetylene (PA) is the simplest conjugated polymer. It can exist in cis- and trans-forms (*cis*- and *trans*-PA isomers). The latter is thermodynamically more stable. The transition between C–C and C = C bonds in *trans*-PA does not require energy change, so the Peierls distortion[3] opens up a substantial gap in the Fermi level. This twofold degeneration leads to the formation of mobile solitons with a length of ≈ 15 C–C units and spin $S = \frac{1}{2}$ on *trans*-PA chains. These correspond to a break in the pattern of bond alternation,[4] and thus determine the fundamental properties of the polymer.

Poly(*p*-phenylene) (PPP), polythiophene (PT), polypyrrole (PP), polyaniline (PANI), and poly(tetrathiafulvalene) (PTTF) are other conductive polymers with pentameric and hexameric unit rings in which two neighboring units are tilted with respect to one another by a torsion angle, for example, equal in PPP to ≈ 23°.[5] This angle is a compromise between the effect of conjugation and crystal-packing energy, which would lead to a planar conformation, and the steric repulsing between *ortho*-hydrogen atoms, which would lead to a non-planar conformation. For these polymers a resonance form can also be derived, which corresponds to a quinoid structure; however, in contrast to *trans*-PA, benzenoid and quinoid forms are not energetically equivalent, with the quinoid structure being substantially higher in energy. As a result, the solitons are trapped in the slightly doped PPP by the charges in polymer structure and the other mobile nonlinear excitations, namely polarons, are formed.[6] These quasiparticles, with the size of about five polymer units,[7] possess an elemental charge e and spin $S = \frac{1}{2}$. With increase of the doping level y (the number of the dopant molecules per polymer unit), the polaron pairs can combine to form spinless bipolarons with charge 2e.

Some of the most studied conductive polymers, as well as nonlinear quasiparticles formed in their chains, are schematically shown in Fig. 1.

A highly anisotropic quasi-one-dimensional (Q1D) π-conjugated structure with the above topological distortions as charge carriers makes such systems fundamentally different from traditional inorganic semiconductors, for example, silicon and selenium, and insulating polymers, for example, polyethylene. Their direct current (dc) conductivity σ_{dc} can be controlled by chemical or electrochemical oxidation or reduction from the insulator to the semiconductor and then to the metal.[1]

The electronic properties of conductive polymers correlate with their structure, morphology, and quality, as well as with the nature and number of the dopant molecules introduced into the polymer matrix.

Different methods were widely used for the study of fundamental structure and dynamics properties of conductive polymers: optical and X-ray photoelectron spectroscopy, scanning electron microscopy (SEM), chromatography, *dc* and alternating current (ac) conductometry, microwave dielectrometry, Faraday balance and alternating force magnetometry, and thermoelectric power.[1,2] As the electronic properties of

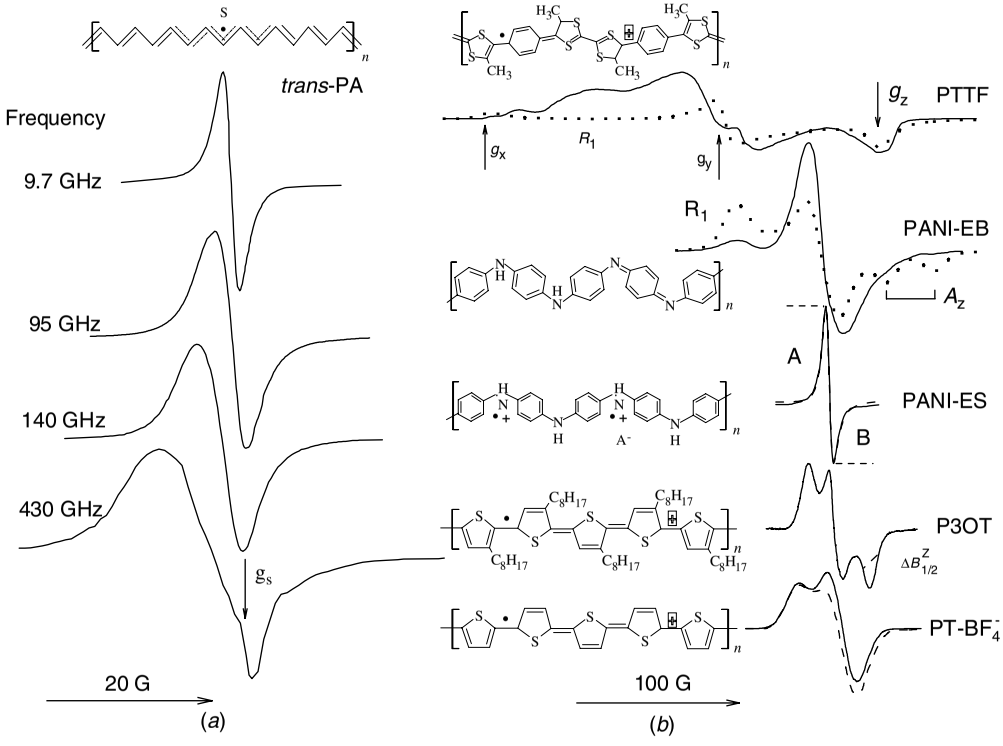

Fig. 1. (*a*)The ESR spectra of *trans*-PA registered at different frequencies at room temperature. (*b*) The D-band ESR spectra of PTTF with $y = 0$ (dotted line) and 0.08 (solid line), PANI-EB whose R_1 PC is shown by dotted line, PANI-ES (in the formula A^- is an anion, and dashed lines show the spectrum calculated from Eq. 5 with D/A = 0.39 and $\Delta B_{pp} = 4.89$ G), P3OT, and PT-BF_4^- registered at $T = 300$ (solid line) and 200 K (dashed line). The components of anisotropic *g*-factors of PC stabilized in the samples are summarized in Table 1. The soliton *S* in *trans*-PA and the polaron in other conductive polymers spread out over a larger number of units than shown schematically here. [From Refs. 12(b), 19, 24, 30(b), 44(b), and 45(a) with permission.]

conductive polymers are related to the existence of nonlinear excitations possessing electron and nuclear spins, various magnetic resonance methods, such as nuclear magnetic resonance (NMR), electron–nuclear double resonance (ENDOR), electron spin–echo envelope modulation (ESEEM), and ESR were also used for the study of these systems.[8,9] Electron spin resonance spectroscopy has the ability to analyze directly the nature and dynamics of nonlinear charge carriers stabilized in conductive polymers.

The ESR investigations are usually carried out at a frequency of $\omega_e/2\pi = \nu_e \leq 10$ GHz and a field $B_0 \leq 3.4$ kG. However, these conditions result in single-line spectra with information limited to the concentration and line width of the paramagnetic centers (PC). In addition, strong cross-relaxation of PC exists at low magnetic fields.[10] Thus, the ESR study of organic conductive systems at $\nu_e \leq 10$ GHz faces considerable limitations.

It was shown[11,12] that the measurement of organic radicals in different solids, especially in conductive polymers at D-band ESR ($\omega_e/2\pi \approx 140$ GHz and $B_0 \approx 50$ kG) enables the absolute sensitivity, precision, and informativity of the method to increase considerably. At high frequencies, the main advantage of the method is the higher spectral resolution of the g-factor due to the basic relation $g_i - g_e \propto \omega_e$ (here, $g_e = 2.00232$ is the g-factor for a free electron). The transition to D-band widens the range of molecular motions in condensed systems by more than an order of magnitude. This sensitivity of the ESR method, that is, the minimum number of spins detected, increases with the increase of ω_e as $N_{min} \propto \omega_e^{-\alpha}$, where $\alpha \approx 0.5$–4.5.[13] Finally, the probability P_{cr} of cross-relaxation (cr) of PC decreases strongly with the increase of a polarizing microwave quantum energy $h\omega_e \propto B_0$ as $P_{cr} \propto \exp(-B_0^2)$,[14] so the spin packets become noninteracting at D-band ESR, and therefore can be saturated at lower values of the magnetic term B_1 of polarizing microwave radiation. The electron relaxation time of PC stabilized in some solids can increase with an increase in ω_e, which is another reason for the appearance of fast passage effects that make an efficient study of their relaxation and dynamics properties possible.

In our laboratory, ESR studies at D-band have investigated the structure, dynamics, and other specific characteristics of PC and their local environment in various biological[11] and conductive[12,15] polymers. The main results for conductive polymers are summarized in this chapter.

2. MAGNETIC PARAMETERS OF CHARGE CARRIERS IN CONDUCTIVE POLYMERS

Trans-PA can be obtained by thermal, chemical, or electrochemical treatment of *cis*-PA.[16] Such a treatment leads to the increase of the polymer dc conductivity σ_{dc} from $\approx 10^{-12}$ up to 10^{-5} S cm^{-1} and is accompanied by the increase in spin concentration from $\approx 10^{18}$ up to 10^{19} spin g^{-1} and by strong line narrowing.[8]

Numerous ESR studies of the nature, composition, relaxation, and dynamics of PC in *cis*- and *trans*-PA were carried out at convenient $\omega_e/2\pi \leq 10$ GHz.[8] Figure 1 exhibits the X-band ($\omega_e/2\pi = 9.7$ GHz) ESR spectra of *trans*-PA as an example: a single symmetric line with effective $g = 2.0026$ and line width $\Delta B_{pp} = 2.2$ G. A small

ESR line width broadening (0.5 G) was observed on cooling to 77 K, probably due to a smaller libration motion of different parts of the polymer chains. The data obtained have no simple interpretation because at this frequency it is impossible to discern the difference between localized and mobile π -radicals with close magnetic parameters.

The increase of the frequency ω_e leads to a change in the line shape, as shown in Fig. 1*a*.[17–19] Analysis of the spectra shows[19] that two PCs are stabilized in *trans*-PA, namely, neutral solitons pinned on short polymer chains with $g_\perp = 2.00283$ and $g_\parallel = 2.00236$, and those moving along the long polymer axis with $g = 2.00269$ and relative contributions of 1.1×10^{-3}:6×10^{-5} spins per carbon atom, respectively. The latter value is two orders of magnitude smaller than that reported by Goldberg[20]. By replacing hydrogen atoms with SR-groups (R is alkyl substitute), that is, the transition from *trans*-PA to poly(bis-alkylthioacetylene) (PATAC), causes a drastic increase in the anisotropy of magnetic parameters of the polymer.[21]

The $g_\perp$ value of *trans*-PA differs from g_e by $g_\perp - g_e = 5 \times 10^{-4}$. According to a perturbation theory,[22] the shift of the *g*-factor is

$$g_{x,y} - g_e = \frac{g_e \rho(0) \lambda}{\Delta E n - \pi^*, \sigma - \pi^*} \tag{1}$$

where ρ(0) is the spin density at the nucleus position, λ is the spin–orbit coupling constant, $\Delta E_{n-\pi^*}$ and $\Delta E_{\sigma-\pi^*}$ are the energies of the unpaired electron $n \rightarrow \pi^*$ and $\sigma \rightarrow \pi^*$ transitions, respectively. Therefore, the difference obtained corresponds to an unpaired electron excitation from the σ_{c-c} orbital to an antibonding π* orbital with $\Delta E_{\sigma-\pi^*} = 14$ eV, which is near $\Delta E_{\sigma-\pi^*} = 14.5$ eV calculated for a normal C–C bond in π-conducting systems.[23] The isotropic *g*-factors of delocalized PC lies near to that of the pinned one. This is evident from the averaging of the **g** tensor components of delocalized solitons due to their mobility with the rate[13]

$$D_{ID}^0 \geq \frac{(g_\perp - g_e)\mu_B B_0}{\hbar} \tag{2}$$

that exceeds 10^9 rad s^{-1} in *trans*-PA.

Figure 1*b* also exhibits a typical D-band ESR spectra of both neat and iodine-doped PTTF sample with more pronounced anisotropic magnetic parameters.[24,25] This polymer with methyl (Me) and ethyl (Et) substituents in which TTF units with R = H, Me, or Et are linked via phenyl (PTTF-R-Ph) or tetrahydroanthracene (PTTF-THA) bridges is a *p*-semiconductor with dc conductivity $\sigma_{dc} \approx 10^{-4}$–$10^{-3}$ S cm^{-1}.[26] The anisotropic ESR spectrum of localized PC R_1 in, for example, PTTF-Me-Ph, is characterized by *g*-factors presented in Table 1. In addition, more mobile polarons R_2 with $g_x = 2.00928$, $g_y = 2.00632$, $g_z = 2.00210$ also appear upon polymer doping. The spectrum of PTTF-Et-Ph was analyzed in terms of two contributions, of localized PC R_1 with magnetic parameters presented in Table 1, and PC R_2 with a nearly symmetric spectrum and $g_{eff} = 2.00706$ diffusing along the polymer long axis with the rate (see Eq. 2) of $D_{ID}^0 \geq 3 \times 10^{10}$ rad s^{-1}. The main components of the *g*-tensor of PC R_1 localized in PTTF–THA are summarized in Table 1 as well. The spectrum of delocalized PC R_2 have $g_\parallel^p = 2.00961$ and

$g_{\perp}^{p} = 2.00585$ (R_2). The concentration ratio $[R_1]/[R_2]$ is 20:1 in PTTF–Me–Ph, 3:1 in PTTF–THA, and 1:1.8 in iodine-doped PTTF–Et–Ph.

Polaron motion along the polymer chain induces interactions between electron spins and between electron and proton spins, which depend on the frequency.[27] The line width of the ESR spectral components of polarons immobilized and delocalized in, for example, PTTF–Et–Ph, increases from 2.8 to 3.8 G and then to 39 G, and from 10.2 to 11.5 and then to 175 G, when the microwave frequency increases from 9.5 to 37, and then to 140 GHz, respectively, at room temperature.[24] It is then possible to determine a real line width of these PCs at the $\omega_e \rightarrow 0$ limit, 2.4 and 8.3 G, respectively.

Polythiophene and its derivatives, poly(3-alkylthiophenes) (P3AT), with sulfur in the backbone are a suitable system for understanding the electronic and optical properties of Q1D systems with nondegenerate ground states.[28] Normally, these compounds are semiconductors, whose mid-gap is determined by the presence of the π-orbital conjugation along the main polymer axis. The presence of polarons in polythiophene and its derivatives was revealed by optical absorption measurements and ESR spectroscopy.[8] At X-band ESR pristine PT and P3AT have a single symmetric line with $g \approx 2.0026$ and $\Delta B_{pp} \approx 4$–8 G, evidencing that the spins do not belong to a sulfur-containing moiety and are localized on the polymer chains.[8]

The D-band ESR spectra of PT and P3OT are more informative.[29,30] The D-band ESR spectrum of P3OT is a superposition of Gaussian and Lorentzian lines with the anisotropic g-factor typical for PC in some other conductive polymers with heteroatoms.[12] The main components of the g-tensor of PC in P3OT are presented in Table 1. The structure of a polymer should affect the distribution of an unpaired electron in polaron, changing the principal values of the PC g-tensor and hyperfine structure. The lower limit of the polaron motion in P3OT can be determined from the shift of the g_x and g_y values compared to g_e, by using Eq. 1 with $\lambda_s = 0.047$ eV to be $D_{ID}^{0} \geq 3.4 \times 10^9$ rad s^{-1}.

In contrast to X-band ESR, the high spectral resolution achieved at D-band ESR allows us to register the structure and/or dynamic changes in all spectral components separately. Fig. 2 shows that the g_x and g_y values clearly reflect the properties of the radical microenvironment. These values of the initial P3OT decrease with the

Table 1. Principal g-Tensor Components g_i and Averaged g-Factors of PC in Conductive Polymers Determined from D-Band ESR at Room Temperature

Sample	g_x	g_y	g_z	$<g>$
PTTF-Me-Ph	2.01189	2.00544	2.00185	2.00639
PTTF-Et-Ph	2.01424	2.00651	2.00235	2.00770
PTTF-THA	2.01292	2.00620	2.00251	2.00721
P3OT	2.00409	2.00332	2.00235	2.00325
PANI-SA	2.00603	2.00382	2.00239	2.00408
PANI-HSA	2.00522	2.00401	2.00228	2.00384

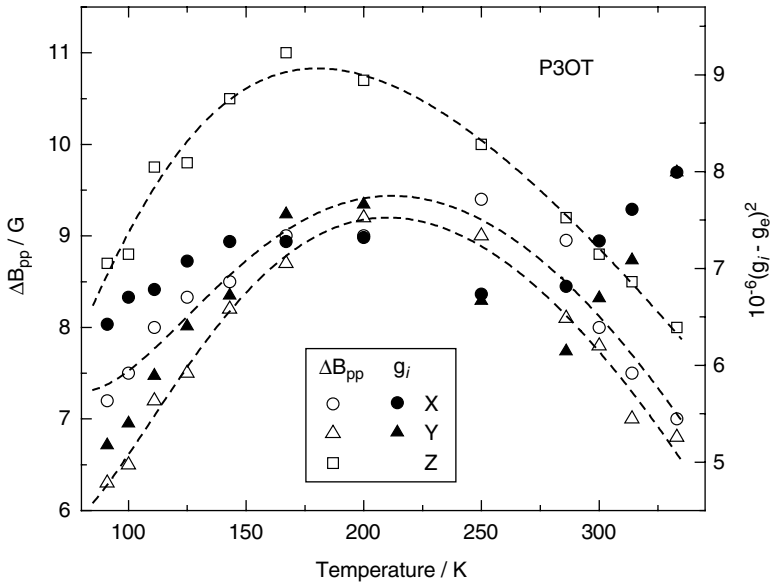

Fig. 2. Temperature dependence of the line width of the main spectral components, and of the squared shifts of g_x and g_y from $g_e = 2.00232$ for P3OT at D-band. From the top down, the dashed lines show the dependences calculated from Eq. 3 with $\Delta B^0_{pp} = 7.3$ G, $\omega^0_{hop} = 8.7 \times 10^{14}\ s^{-1}$, $E_a = 0.014$ eV, $J_d = 0.30$ eV, $\Delta B^0_{pp} = 12.3$ G, $\omega^0_{hop} = 1.8 \times 10^{14}\ s^{-1}$, $E_a = 0.022$ eV, $J_d = 0.29$ eV, and $\Delta B^0_{pp} = 8.7$ G, $\omega^0_{hop} = 8.5 \times 10^{14}\ s^{-1}$, $E_a = 0.020$ eV, $J_d = 0.27$ eV. [From Ref. 30(b) with permission.]

temperature decrease from 333 down to 280 K, possibly due to the transition to a more planar conformation of the polymer chains. Below 280 K, these values increase at the sample freezing down to 160–220 K, and then decrease with a further temperature decrease. The decrease of g_x and g_y values at low temperatures can be explained by a harmonic vibration of macromolecules that reflects the crystal-field modulation and is characterized by the $g(T) \propto T$ dependence.[31] At the same time, the line width of the P3OT spectral components increases with a temperature increase from 90 K up to the phase transition characteristic temperature $T_c \approx 200$ K, and then decreases as the temperature increases. This effect of the line width decrease below T_c can be due to molecular motion of alkyl groups and/or acceleration of relaxation processes. If one assumes that molecular dynamics and/or electron relaxation lead to broadening of the X, Y, and Z spectral components, the respective activation energies 3.6, 4.9, and 4.3 meV are determined from the slopes of these dependences at $T \geq T_c$.

The extremal variation of the line width can be interpreted in the framework of the Houzé–Nechtschein model[32] of dipole–dipole interaction between different PC. According to this model, the collision of mobile PC with other spins should broaden ESR lines as

$$\Delta B_{pp} = \Delta B^0_{pp} + \delta(\Delta B_{pp}) = \frac{16\omega_{hop}C}{27\gamma_e}\left(1 + \frac{\hbar^2\omega^2_{hop}}{144\, J^2_d}\right) \qquad (3)$$

where ΔB_{pp}^{0} is the line width of noninteracting polarons, ω_{hop} is the frequency of the polaron hopping along a polymer chain, C is the number of guest PC per aniline ring, and J_d is the constant of the spin dipole–dipole interaction in the system. If the ratio $J_d/\hbar$ exceeds the frequency of collision of both PC types, the condition of strong interaction is realized in the system that leads to a direct relation of the spin-spin interaction and polaron diffusion frequencies, so that $\lim[\delta(\Delta B_{pp})] = \frac{16}{27} C\omega_{hop}$. In an opposite case, if the condition of weak interaction prevails, the result is an inverse dependence of these frequencies, $\lim[\delta(\Delta B_{pp})] = \frac{4}{3} (C/\omega_{hop})(J_d/\hbar)^2$. According to the spin exchange fundamental concepts,[33] the extreme $\delta(\Delta B_{pp})(T)$ dependence should reflect both types of spin–spin interaction, at $T \leq T_c$ and $T \geq T_c$, respectively. An additional plausible reason for line broadening can be higher spin localization with a temperature decrease at $T \geq T_c$.

Assuming an activation character of the spin–spin interaction with activation energy E_a, when $\omega_{hop} = \exp(-E_a/k_B T)$, the temperature dependence of the line widths for the X, Y, and Z spectral components can be calculated from Eq. 3 with E_a = 0.022, 0.020, and 0.014 eV, respectively (Fig. 2). The $J_d \approx 0.3$ eV value obtained exceeds the corresponding spin-exchange constant for nitroxide radicals with paramagnetic ions, $J_d \leq 0.01$ eV.[34]

The data presented in Fig. 2.3 evidence that the correlation of line width with the spin–orbit coupling according to the Elliot mechanism is [35]

$$\sigma \propto \Delta B_{pp}^{-1} = \frac{\tau_s}{\alpha(g-g_e)^2} \tag{4}$$

where σ is the conductivity, α is the constant, g–$g_e \propto \lambda/\Delta E_{i-\pi^*}$ is the shift of the g-factor, and τ_s is the electron scattering time. Such a mechanism plays an important role in the charge transfer in organic ion–radical salts[36] and conductive polymers with pentameric rings.[8] Indeed, $\Delta B_{pp}^{x} \propto \Delta g_x^2$ and $\Delta B_{pp}^{y} \propto \Delta g_y^2$ dependences are valid for P3OT at least at $T \leq T_c$. This means that different mechanisms affect the individual components of the P3OT spectrum, and that the scattering of charge carriers (see below) should be governed by the potential of the polymer backbone.

PANI differs from other conducting polymers in several important aspects. In contrast to PA- and PPP-like polymers, it has no charge conjugation symmetry. Besides, both phenyl rings and nitrogen atoms are involved in polymer conjugation. The rings of PANI can rotate or flip, significantly altering the nature of electron–phonon interaction in this polymer. During doping of PANI or transition from its emeraldine base form (PANI-EB) to emeraldine salt (PANI-ES), its conductivity increases by > 10 orders of magnitude, whereas the number of electrons on the polymer chains remains constant in the PANI-ES.[37–41] Such doping is accompanied by appearance of the Pauli susceptibility,[38,39] characteristic for classic metals, due to formation of high-conductive completely protonated or oxidated clusters with a characteristic size of $\approx$ 5 nm in amorphous polymer.[40] In some cases, diamagnetic bipolarons[41] and/or antiferromagnetic interacting polaron pairs,[42] each possessing two elemental charges, can also be formed in heavily doped polymer.

PANI-EB and PANI-ES doped with surfuric (PANI-SA), hydrochloric (PANI-HCA), camphorsulfonic (PANI-CSA), 2-acrylamido-2-methyl-1-propanesulfonic

(PANI-AMPSA), and *p*-toluenesulfonic (PANI-PTSA) acids up to $y \leq 0.60$ were also studied in detail by multifrequency ESR.[25,43–48]

Figure 1 shows typical D-band ESR spectra of PANI-EB and PANI-ES samples. The analysis of the data obtained showed that two types of PC are stabilized in PANI-SA: polarons R_1 localized on short polymer chains, –(Ph–HN^{+*}–Ph)–, with $A_x = A_y = 4.5$ G, $A_z = 30.2$ G, and *g*-factors presented in Table 1; and polarons R_2 with $g_\perp = 2.00439$ and $g_\parallel = 2.00376$ moving along the polymer chains with a rate (see Eq. 2) $D^0_{ID} = 6.5 \times 10^8$ rad s^{-1}. Assuming a McConnell proportionality constant for the hyperfine interaction of the spin with nitrogen nucleus $Q = 23.7$ G,[49] a spin density is estimated on the heteroatom nucleus of $\rho_N(0) = (A_x + A_y + A_z)/(3Q) = 0.55$. The lowest excited states of the localized PC were determined from Eq. 1 to be $\Delta E_{n\pi^*} = 2.9$ eV and $\Delta E_{\sigma\pi^*} = 7.1$ eV at $\rho^\pi_N = 0.56$.[50] In PANI-HCA, R_1 also demonstrates the strongly anisotropic spectrum with the principal components of the *g*-tensor summarized in Table 1, and hyperfine coupling constant $A_z = 22.7$ G. For radicals R_2 $g_\perp = 2.00463$ and $g_\parallel = 2.00223$.

Highly doped PANI,[44,45,47,48] PT,[29] PPP,[51] and other conductive polymers demonstrate a Dyson-like[52] spectra with the line asymmetry factor *A*/*B* (Fig. 1) due to the formation of a skin layer on the polymer surface at D-band ESR. This effect was also detected at $\omega_e/2\pi \leq 10$ GHz.[8] The above line shape distortion is accompanied by its shift to higher magnetic fields; therefore, in order to determine correctly all the magnetic parameters, both the *A* and *D* terms should be considered.

Generally, the first derivative of the Lorentzian line can be calculated as

$$\frac{d\chi}{dB} = A\,\frac{2x}{(1+x^2)^2} + D\,\frac{1-x^2}{(1+x^2)^2} \tag{5}$$

where $x = 2(B\text{-}B_0) / \sqrt{3}\Delta B^L_{pp}$. The line asymmetry *A*/*B* (see Fig. 1) correlates with *A* and *D* coefficients of Eq. 5 as $A/B = 1 + 1.45\ D/A$.

The PC stabilized in PT-BF^-_4 has an axially symmetric D-band ESR spectrum with $g_\parallel = 2.00412$, $g_\perp = 2.00266$, $\Delta B_{pp} = 15.2$ G, $\Delta E_{\sigma\text{-}\pi^*} = 4.0$ eV, typical for a radical localized on a polymer backbone (Fig. 1). The ClO^-_4 doped PT is characterized by $g_\parallel = 2.00230$, $g_\perp = 2.00239$, $\Delta B_{pp} = 26.3$ G, and $\Delta E_{\sigma\text{-}\pi^*} = 7.1$ eV.[29]

As the doping level *y* of PANI-SA exceeds 0.21, the *g*-factor of PC R_2 becomes isotropic and decreases from $g_{R2} = 2.00418$ down to $g_{iso} = 2.00314$. This effect is accompanied by a narrowing of the R_2 ESR spectrum, and was explained by a depinning of Q1D spin diffusion along the polymer chain and formation of the areas with high spin density in which a strong exchange of spins on neighboring chains occurs. This is in agreement with the assumption[40] of formation in amorphous PANI-EB of metal-like domains with Q3D delocalized electrons.

Doping of conducting polymers leads to the increase of the paramagnetic susceptibility, χ. This parameter consists of the temperature-independent Pauli susceptibility of the Fermi gas χ_P, a temperature-dependent contribution of localized Curie PC χ_C, and the term χ_{ST} "becoming" due to a possible singlet–triplet spin equilibrium in the system,[53]

$$\chi = \chi_P + \chi_C + \chi_{ST} = N_A\mu^2_{eff}n(\varepsilon_F) + \frac{N_s\mu^2_{eff}}{3k_BT} + \frac{k_1}{T}\left[\frac{\exp(-J/k_BT)}{1 + 3\exp(-J/k_BT)}\right]^2 \tag{6}$$

where N_A is the Avogadro's number, N_s is a number of spins with $S=\frac{1}{2}$, $\mu_{eff}=\mu_B g\sqrt{S(S+1)}$ is the effective magneton, k_B is the Boltzmann constant, $n(\varepsilon_F)$ is the density of states per unit energy (eV) for both spin directions per monomer unit at the Fermi level ε_F, $N_s/3k_B=C$ is the Curie constant per mol-C(mol-monomer)$^{-1}$, k_1 is a constant, and J is the antiferromagnetic exchange coupling constant.

For example, PC in PANI-SA demonstrates the extreme temperature dependence of the effective paramagnetic susceptibility (Fig. 3). As in the case of polyaniline perchlorate,[54] this indicates a strong antiferromagnetic spin interaction due to a singlet–triplet equilibrium included in the total paramagnetic susceptibility. Indeed, Fig. 3 shows that the paramagnetic susceptibility experimentally determined for the PANI-SA samples is well reproduced by Eq. 6 with $J \geq 0.051$ eV. The J value is close to that obtained for the ammonia treated PANI.[54] Note that $n(\varepsilon_F) = 0.9$–1.4 states per electroviolet per one ring determined for PANI-SA, is consistent with the value determined earlier for PANI heavily treated with other dopants.[55,38] With assumption of a metallic behavior, one can estimate that the energy of N_P Pauli spins,[56] $\varepsilon_F = 3N_p/2n(\varepsilon_F)$, for example in PANI-ES with $0.21 \leq y \leq 0.53$, will be 0.1–0.51 eV.[44] This value is close to that (0.4 eV) obtained, for example, for PANI-CSA.[57] From this value, the number of charge carriers with mass $m_c = m_e$ in heavily doped PANI-SA, $N_c = (2m_c\varepsilon_F/\hbar^2)^{3/2}/3\pi^2$,[56] is evaluated to be 1.7×10^{21} cm^{-3}. The

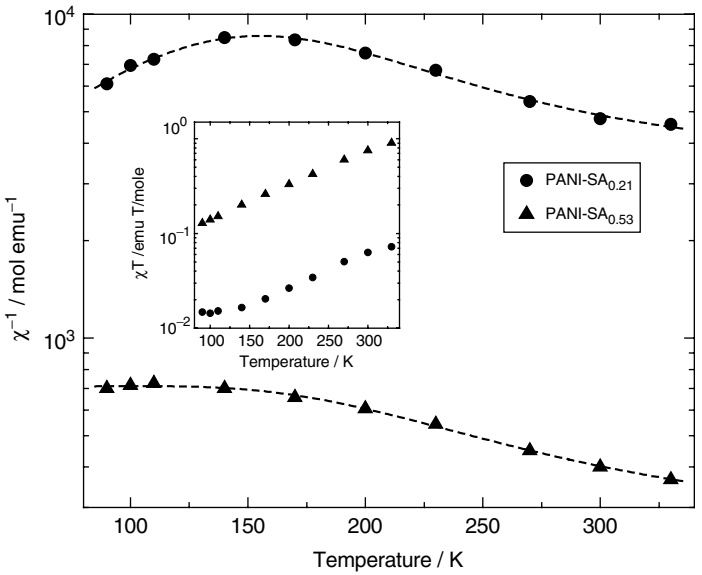

Fig. 3. Temperature dependence of inverse paramagnetic susceptibility and χT product (inset) of PANI-SA samples with different doping levels. Upper and lower dashed lines show the dependences calculated from Eq. 6 with, respectively, $\chi_P = 3.1 \times 10^{-5}$ emu mol^{-1}, $C = 1.2 \times 10^{-2}$ emu K mol^{-1}, $k_1 = 4.2$ emu K mol^{-1}, $J = 0.051$ eV, and $\chi_P = 1.4 \times 10^{-3}$ emu mol^{-1}, $C = 1.6 \times 10^{-2}$ emu K mol^{-1}, $k_1 = 48.6$ emu K mol^{-1}, $J = 0.057$ eV. [From Refs. 12(b) and 45(a) with permission.]

value obtained is close to a total volume spin concentration in PANI-SA. This fact leads to the conclusion that all PC take part in polymer conductivity. For heavily doped PANI-SA samples, the concentration of spin charge carriers is less than that of spinless ones, due to the possible collapse of pairs of polarons into diamagnetic bipolarons. The velocity of the charge carrier near the Fermi level, $v_F = 2c_{1D}/\pi n(\varepsilon_F)$,[56] can then be calculated, $v_F = (3.3–7.2) \times 10^7$ cm s^{-1}. Note that the paramagnetic susceptibility depends weekly on the measuring frequency; therefore this parameter for other conductive polymers is discussed only in general terms.

3. RELAXATION AND DYNAMICS OF CHARGE CARRIERS IN SLIGHTLY DOPED CONDUCTIVE POLYMERS

The line width of mobile PC in PANI-AMPSA$_{0.6}$ depends on ω_e: $\Delta B_{pp}(\omega_e) = 1.5 + 6.5 \times 10^{10}\omega_e^{-0.84}$ G at room temperature. As in the case of other polymers, it is possible to estimate a correct line width at the $\omega_e \to 0$ limit and to reveal the dependence of spin–spin relaxation time on the microwave frequency. As emphasized above, the cross-relaxation between spin packets decreases drastically at high magnetic fields and causes saturation at lower values of B_1. This effect can be used for the study of relaxation and dynamics parameters of PC in different solids,[11] conducting polymers among them.[12]

Generally, the first derivative of a dispersion signal U is[58]

$$U(\omega_e t) = u_1 g'(\omega_e)\sin(\omega_e t) + u_2 g(\omega_e)\sin(\omega_e t - \pi) + u_2 g(\omega_e)\sin(\omega_e t \pm \pi/2) \quad (7)$$

where u_1, u_2, and u_3 are, respectively, the in-phase and quadrature dispersion terms with $g(\omega_e)$ shape.

Figure 4 shows changes of in-phase and quadrature terms of the dispersion signal of PC in *cis*-PA at different B_1 values and in P3OT at different temperatures. The relaxation times of adiabatically saturated PC in these and other π-conductive polymers can be determined separately from the analysis of the u_i terms of Eq. 7 as[18]

$$T_1 = \frac{3\omega_m(1 + 6\Omega)}{\gamma_e^2 B^2{}_{1_0}\Omega(1 + \Omega)} \quad (8a)$$

$$T_2 = \frac{\Omega}{\omega_m} \quad (8b)$$

(here $\Omega = u_3/u_2$, B_{1_0} is the polarizing field at which the condition $u_1 = -u_2$ is valid) at $\omega_m T_1 > 1$ and

$$T_1 = \frac{\pi u_3}{2\omega_m u_1} \quad (9a)$$

$$T_2 = \frac{\pi u_3}{2\omega_m(u_1 + 11u_2)} \quad (9b)$$

at $\omega_m T_1 < 1$.

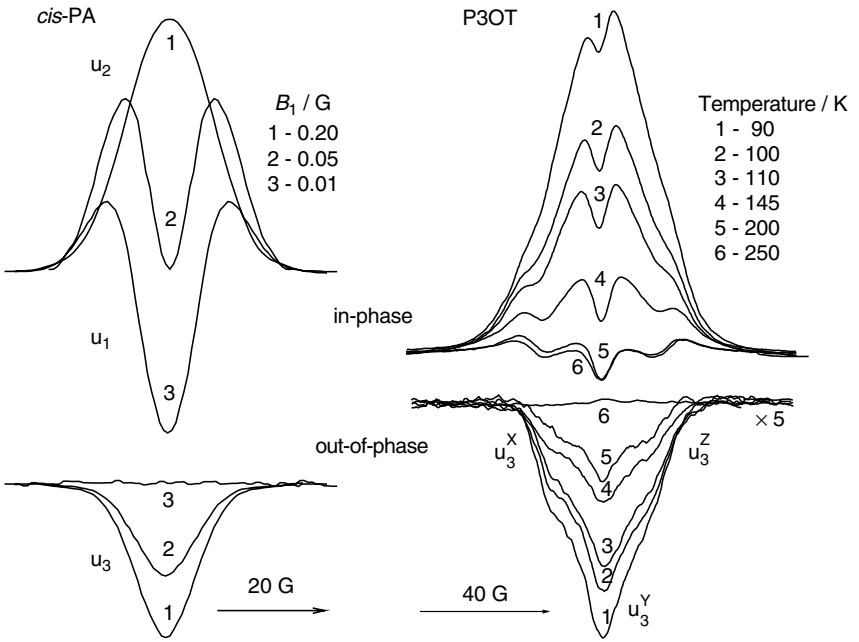

Fig. 4. The D-band in-phase and π/2-out-of-phase dispersion ESR spectra of *cis*-PA registered at different B_1 values and room temperature, and for P3OT registered at different temperatures and B_1 = 0.2 G (*6*). [From Refs. 12(b) and 30(b) with permission.

The inequalities $\omega_m T_1 > 1$ and $\omega_m T_1 < 1$ hold for *cis*- and *trans*-PA, respectively,[59] therefore their T_1 and T_2 values can be calculated by using Eq. 8 and 9, respectively. Fig. 5 exhibits these parameters for solitons in *trans*-PA with randomly oriented and with partly stretch-oriented polymer chains as a function of temperature and the angle ψ between the external magnetic field B_0 and the stretching directions. Figure 5 shows the field sensitivity of the relaxation parameters of solitons that can be explained by the depinning of their motion in *trans*-PA film.

Such spin diffusion along and between polymer chains, respectively, with coefficients D_{1D} and $D_{3D,}$ (where 1D = one dimensional and 3D = three dimensional) induces an additional magnetic field onto other electron and nuclear spins and, therefore, should accelerate both the relaxation times of the whole spin reservoir. Dipole–dipole interaction between equal spins prevails in conductive polymers, so the relaxation rates can be calculated as[22,60]

$$T_1^{-1} = \langle \Delta\omega^2 \rangle \, [2J(\omega_e) + 8J(2\omega_e)] \tag{10a}$$

$$T_2^{-1} = \langle \Delta\omega^2 \rangle \, [3J(0) + 5J(2\omega_e)] \tag{10b}$$

where $<\Delta\omega^2>$ is the averaged constant of dipole–dipole spin interaction in a powder-like sample and $J(\omega_e) = (2D_{1D}\omega_e)^{-1/2}$ at $D_{3D} \leq \omega_e \leq D_{1D}$ or $J(\omega_e) = (2\, D_{1D}D_{3D})^{-1/2}$

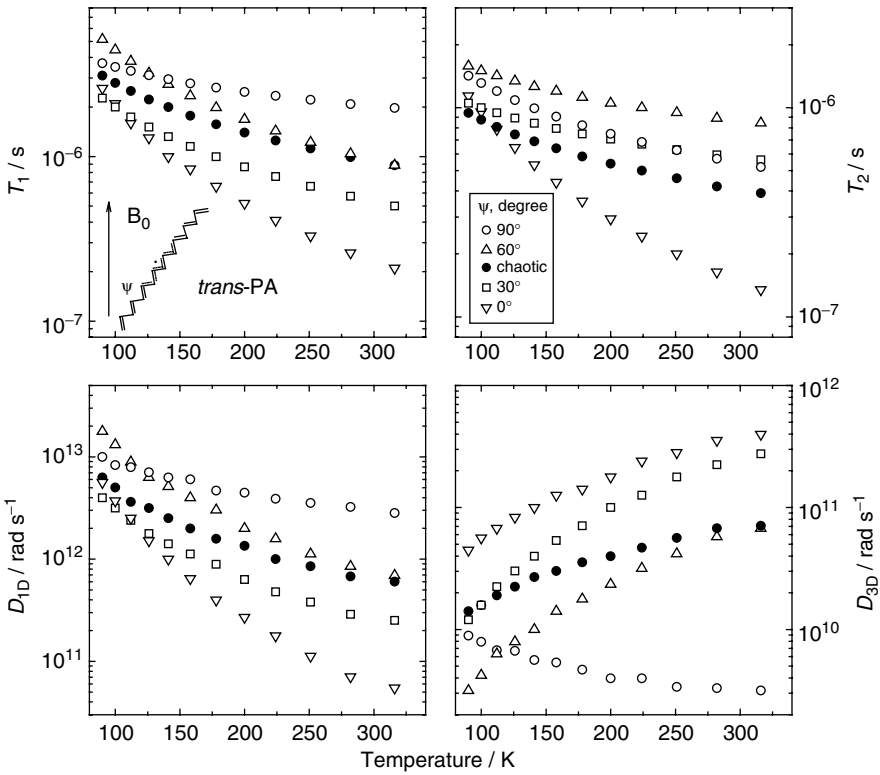

Fig. 5. Temperature dependence of effective spin–lattice T_1 and spin–spin T_2 relaxation times calculated from Eqs. 8 as well as of intrachain D_{1D} and interchain D_{3D} diffusion rates calculated from Eq. 10 for neutral solitons diffusing in *trans*-PA along and between randomly oriented chains and chains oriented with their *c*-axis with respect to an external magnetic field by $\psi = 90^0$, 60^0, 30^0, and 0^0. [From Refs. 12(b) and 61 with permission.]

at $\omega_e \leq D_{3D}$ is the spectral density function for a spin motion in a Q1D system. These equations become more complex in the case of an oriented polymer system.

Fig. 5 displays the temperature dependencies of the D_{1D} and D_{3D} coefficients calculated for the soliton diffusion in *trans*-PA with randomly oriented and partly stretch-oriented chains. This figure shows that, as in the case of relaxation parameters, both the 1D and 3D diffusion rates are sensitive to the orientation of the polymer chains in an external magnetic field due to soliton diffusion in this Q1D system. The $D_{1D}(\psi)$ function for an oriented sample is opposite to the $D_{3D}(\psi)$ one. Since the main *c*-axes are arbitrarily oriented in an initial *trans*-PA, these values are averaged over angle ψ. Moreover, the averaged D_{1D} value is well described by the equation $<D_{1D}> = D_{1D}^{\perp}\cos^2\psi + D_{1D}^{\parallel}\sin^2\psi$, where $D_{1D}^{\perp}$ and $D_{1D}^{\parallel}$ are the extremes of the $D_{1D}(\psi)$ function. Thus, $D_{1D}^{\perp} \gg D_{1D}^{\parallel}$ inequality displays spin delocalization over N_s soliton sites equal to $\sqrt{D_{1D}^{\perp} / D_{1D}^{\parallel}}$.[61] The analysis of the data presented in Fig. 5 gives $N_s(T) \propto T^{1.0}$ temperature dependence for the soliton width and $2N_s = 14.8$ cell units at room temperature. This value is in good agreement with that theoretically predicted[4] and

experimentally obtained.[62] Extrapolation to the low temperature range allows us to suppose the lowest $T_0 \approx 60$ K, where the soliton width starts to increase. Krinichnyi et al.[61] have shown that a soliton in *trans*-PA is transferred according to the Burgers–Korteweg–de-Vries theory, which described a dynamics of solitary wave in solids.

The ac conductivity of a conductive polymer due to dynamics of N_s spin charge carriers can be calculated from the modified Einstein relation

$$\sigma_{1,3D}(T) = \frac{N_s e^2 D_{1,3D} c_{1,3D}^2}{k_B T} \tag{11}$$

where c_{iD} is the appropriate lattice constant.

Figure 6 exhibits the conductivity due to intra- and interchain soliton diffusion in slightly iodine-doped *trans*-PA. The intrachain charge transfer was analyzed[63] in terms of phonon-assisted spin hopping between soliton sites, in the framework of the Kivelson phenomenological model,[64] with predicted conductivity

$$\sigma_{ac}(T) = \sigma_0 \omega_e T^{-1} \left[1n \frac{k_1 \omega_e}{T^{n+1}} \right]^4 \tag{12}$$

where k_1 is constant. The fitting of experimental data by Eq. 12 confirms the applicability of the Kivelson theory for the explanation of charge transfer by soliton in *trans*-PA.

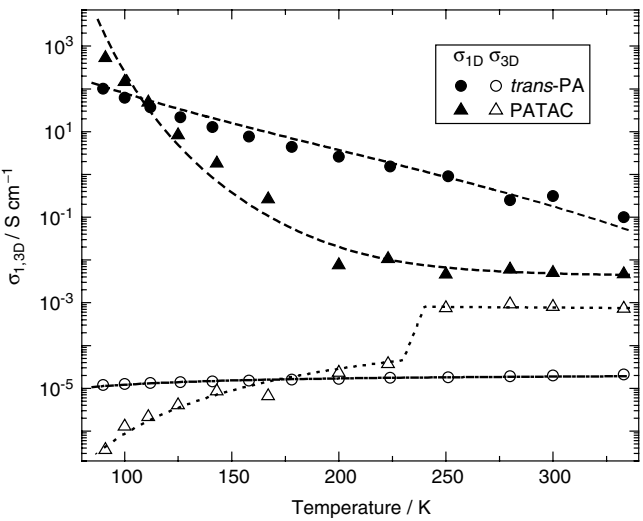

Fig. 6. Temperature dependence of conductivity σ_{1D} and σ_{3D} due to soliton motion in slightly doped *trans*-PA and polaron motion in laser-modified PATAC. The dependences calculated from Eq. 12 with $\sigma_0 = 2.8 \times 10^{-13}$ S s K cm^{-1}, $k_1 = 6.6 \times 10^{14}$ s K$^{14.2}$, and $n = 13.2$ (upper dashed line), Eq. 15 with $\sigma_0 = 2.9 \times 10^{-9}$ S K cm^{-1} and $\hbar\omega_{ph} = 0.18$ eV (lower dashed line), Eq. 14 with $\sigma_0 = 6.5 \times 10^{-20}$ S s (K cm)$^{-1}$ (dash–dotted line), and Eq. 13 with $\sigma_0 = 3.3 \times 10^{-18}$ S s (cm K)$^{-1}$ ($T < 230$ *K*), $\sigma_0 = 5.2 \times 10^{-17}$ S s (cm K)$^{-1}$ ($T > 230$ K) and $E_a = 0.055$ eV (dotted line) are shown as well. [From Refs. 12(b) and 21(b) with permission.]

One can expect that the interchain charge transfer be caused by thermal activation of a soliton to the band tails; therefore[65]

$$\sigma_{ac}(T) = \sigma_0 T \omega_e^{\gamma} \exp\left(-\frac{E_a}{k_B T}\right) \tag{13}$$

Here, γ is a constant that lies normally near 0.3–0.8 for solids and E_a is the energy for activation of charge carrier to extended states. It was deduced[66] that these two values of, for example, poly(3-methylthiophene), correlate as $\gamma = 1 - \alpha k_B T/E_a$ with $\alpha = 1$ and $E_a = 0.18$ eV.

Analysis of data obtained for *trans*-PA has shown, however, that its conductivity follows Eq. 13 at a too small value of E_a. For a better explanation of experimental data, the pair approximation[67] for Q3D charge hopping appeared more suitable. According to this approach, the charge tunneling between random energy electron potential wells governs the ac conductivity,[68]

$$\sigma_{ac}(T) = \frac{1}{3}\,\pi e^2 k_B T n^2 k_B(\varepsilon_F)\,\langle L\rangle^5\,\omega_e \ln^4\left(\frac{\omega_0}{\omega_e}\right) = \sigma_0 T \tag{14}$$

where $<L>$ is the averaged length of charge wave localization function and ω_0 is a hopping frequency.

The comparison of the dependences experimentally obtained and calculated by using Eq. 14 provide evidence for charge tunneling transfer in *trans*-PA (Fig. 6).

The relaxation and electron dynamics properties of this polymer are changed sufficiently as a hydrogen atom is replaced by a sulfur-based alkyl group. Such substitution leads to the stronger temperature dependence of relaxation times in laser-modified PATAC as compared with *trans*-PA.[21]

Figure 6 also shows the contribution of both 1D and 3D polaron motions to the ac conductivity of the laser-modified PATAC. Its intrachain conductivity σ_{1D} was interpreted in terms of the model of the charge-carrier scattering on the lattice optical phonons proposed by Kivelson and Heeger for metal-like clusters in conjugated polymers,[69]

$$\sigma_{ac}(T) = \sigma_0 T\left[\sinh\left(\frac{\hbar\omega_{ph}}{k_B T}\right) - 1\right] \tag{15}$$

where ω_{ph} is the angular frequency of the optical phonon.

The $\sigma_{1D}(T)$ and $\sigma_{3D}(T)$ dependences obtained for PATAC are fairly well fitted by equation 15 with $\hbar\omega_{ph} = 0.18$ eV and Eq. 14 with $E_a = 0.061$ eV, respectively (Fig. 6). The break in the $\sigma_{3D}(T)$ curve can be attributed to a change in the conformation of the system. The energy necessary for the charge-carrier activation hopping between polymer chains is close to the energy of activation of the polymer chain librations (see below). This fact is evidence of the interference of charge transfer and macromolecular dynamics processes in the polymer.

Figure 7 shows the temperature dependence of the relaxation times of polarons in P3OT determined from its dispersion spectrum terms presented in Fig. 4; of the spin diffusion constants D_{1D} and D_{3D}; and of the conductivity due to polaron mobility along σ_{1D} and between σ_{1D} polymer chains.[30]

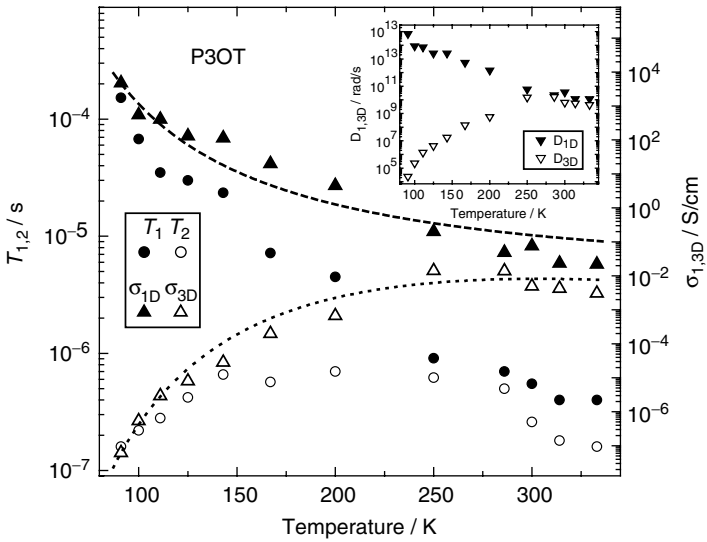

Fig. 7. Temperature dependence of the spin–lattice T_1, spin–spin T_2 relaxation times, intrachain D_{1D} and interchain D_{3D} diffusion rates (inset) of polarons in P3OT and appropriate terms of its ac conductivity. The dashed line shows the dependences calculated from Eq. 15 with $\sigma_0 = 5.5 \times 10^{-8}$ S cm^{-1} K^{-1} and $\hbar\omega_{ph} = 0.13$ eV. The dotted line shows the dependence calculated from Eq. 13 with $\sigma_0 = 9.1 \times 10^{-11}$ S s$^{\gamma}$ cm^{-1} K^{-1}, $\alpha = 2.1$, $E_a = 0.18$ eV. [From Ref. 30(b) with permission.]

The D_{1D} value exceeds the lower limit of the spin motion D^0_{ID} by more than one to two orders of magnitude; however, the D_{3D} value obtained lies near $D \approx 2.1 \times 10^{10}$ s^{-1} evaluated from the charge-carrier mobility in slightly doped P3OT.[70] The anisotropy of spin dynamics D_{1D}/D_{3D} increases from 6 at 300 K up to 2500 at 200 K and up to 3.8×10^8 at 100 K. This leads to the respective increase in the anisotropy of conductivity σ_{1D}/σ_{3D} from 15 up to 6.8×10^3, and then up to 1.0×10^9.

As for the PATAC sample, the charge transfer along the chains in P3OT is characterized by the strong temperature dependence, especially in the low-temperature region (Fig. 7). Such behavior is usually associated with the scattering of charge carriers on the optical lattice phonons. Indeed, the intramolecular ac conductivity is in good agreement and follows Eq. 15 with $\hbar\omega_{ph} = 0.13$ eV. This value is close to that obtained for laser-modified PATAC and also for PANI-ES (see below). On the other hand, the interchain conductivity σ_{3D} increases with the temperature increase at $T \leq 200$ K, and then slightly decreases at higher temperatures. This is typical for the systems with a strong coupling of the charge with the lattice phonons. The γ value in Eq. 13 was shown[66] to depend on the activation energy, E_a, of polaron transfer between P3AT chains, so one can use this approach for the explanation of the 3D conductivity in the P3OT sample as well.

Figure 7 shows that the σ_{3D} term of conductivity of P3OT is well fitted by Eq. 13 with $\alpha = 2.1$ and $E_a = 0.18$ eV. The latter value is close to that determined for poly (3-methylthiophene)[66] and also to the energy of lattice phonons in P3OT determined above.

Relaxation and dynamics properties of charge carriers depend not only on the polymer structure, but also on its doping level. The temperature dependence of effective D_{1D} and D_{3D} calculated from Eqs. 10 for PC in PTTF samples with different structure and iodine content are shown in Fig. 8.[12,24,25] The D_{1D} parameter increases by two orders of magnitude at the transition from PTTF-Et-Ph to PTTF-THA and to PTTF-Me-Ph samples, due probably to a more planar conformation in the chain monomer units or crystallinity in this series.

The σ_{1D} and σ_{3D} conductivity terms of these PTTF samples are presented in Fig. 9 as a function of temperature. It is seen that the most acceptable intrachain charge transfer can be suggested in terms of the Kivelson–Heeger theory of spin–phonon interaction. Figure 9 shows that ac conductivity of the PTTF-Et-Ph and both of the PTTF-THA samples are really fitted by Eq. 15. The σ_{3D} value of the PTTF-Me-Ph$_{0.02}$ sample monotonically decreases with a temperature decrease. On the other hand, this value of PTTF-Me-Ph with $y \geq 0.05$, somewhat increases at the sample cooling from room temperature down to $T_c \approx 180$ K and then decreases on further cooling of the sample (Fig. 9). Such dependence can be explained by the thermally activated interchain polaron hopping in conduction band tails with activation energy E_a. Temperature dependences of conductivity due to such spin motion calculated from Eq. 13 are shown by dotted lines in Fig. 9. The σ_{3D} value increases in PTTF when the Ph group is replaced by THA where THA=tetrahydroanthracene (i.e., PTTF–THA is PTTF in which THF units are linked via tetrahydroanthracene bridges). This fact allows us to conclude that the structure of a polymer governs the polaron mobility and anisotropy of its transfer in PTTF.

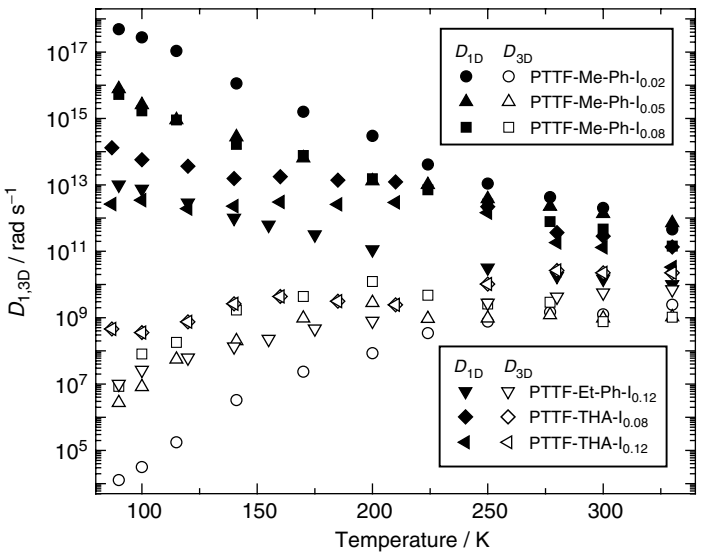

Fig. 8. Temperature dependence of the effective intrachain D_{1D} and interchain D_{3D} polaron diffusion rates in iodine-doped PTTF samples with different doping levels, determined from Eqs. 10. [From Refs. 12(b) and 24 with permission.]

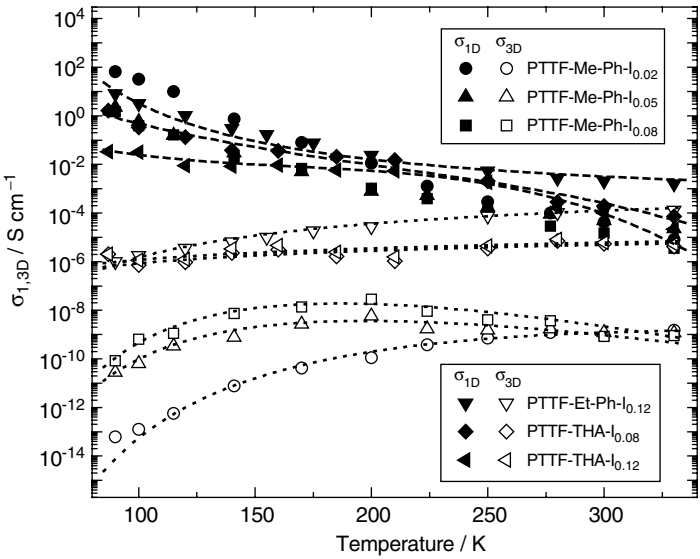

Fig. 9. Temperature dependence of ac conductivity of iodine-doped PTTF due to intrachain and interchain spin motion, calculated from Eq. 11 using data presented in Fig. 8. From the top down, dashed lines show $\sigma_{1D}(T)$ calculated from Eq. 15 with $\sigma_0 = 4.2 \times 10^{-7}$ S cm^{-1} and $h\omega_{ph} = 0.11$ eV, $\sigma_0 = 2.0 \times 10^{-5}$ S cm^{-1} and $\hbar\omega_{ph} = 0.025$ eV, and $\sigma_0 = 4.1 \times 10^{-5}$ S cm^{-1} and $\hbar\omega_{ph} = 0.024$ eV. Top to down dotted lines show $\sigma_{3D}(T)$ calculated from Eq. 13 with $\sigma_0 = 2.7 \times 10^{-17}$ S K^{-1}cm^{-1}s, $\alpha = 0$, $E_a = 0.052$ eV; $\sigma_0 = 1.9 \times 10^{-19}$ S K^{-1}cm^{-1}s, $\alpha = 0$, $E_a = 0.007$ eV; $\sigma_0 = 1.6 \times 10^{-19}$ S K^{-1}cm^{-1}s, $\alpha = 0$, $E_a = 0.09$ eV; $\sigma_0 = 1.1 \times 10^{-13}$ S K^{-1}cm^{-1}s, $\alpha = 3.2$, $E_a = 0.14$ eV; $\sigma_0 = 5.4 \times 10^{-16}$ S K^{-1}cm^{-1}s, $\alpha = 2.1$, $E_a = 0.12$ eV; $\sigma_0 = 1.6 \times 10^{-18}$ S K^{-1}cm^{-1}s, $\alpha = 1.1$, $E_a = 0.16$ eV as well. [From Refs. 12(b) and 24 with permission.]

The Fermi velocity v_F in PTTF samples is near 2×10^7 cm s^{-1}. The mean free path l_i of a charge was determined for the PTTF samples to be $l_i = \nu_{1D} c_{1D}^2 \nu_F^{-1} = 10^{-2}$–$10^{-4}$ nm at room temperature, and l_i is less than the lattice constant a; therefore the charge transfer is incoherent in such a Q1D metal-like polymer.

The temperature dependences of effective D_{1D} and D_{3D} calculated from Eqs. 10 for both types of PC in the PANI-EB and some slightly doped PANI were also determined (Fig. 10).[25,44,45,48] It seems reasonable that the anisotropy of the spin dynamics, being maximal in PANI-EB, decreases as y increases. For $y \geq 0.21$ the dimensionality of PANI-ES grows and the spin motion tends to become almost isotropic. This result disagrees with the results[71] obtained at lower ω_e, which concluded that there was high anisotropy of the spin dynamics in highly HCA-doped PANI even at room temperature.

The strong temperature dependence of the D_{1D} of PC in PANI-EB is a result of multiphonon charge hopping processes due to strong spin–lattice interaction. In contrast to undoped *trans*-PA, a small number of charge carriers exists even in the emeraldine base form of PANI. For this reason, a charge dynamics in the polymer can

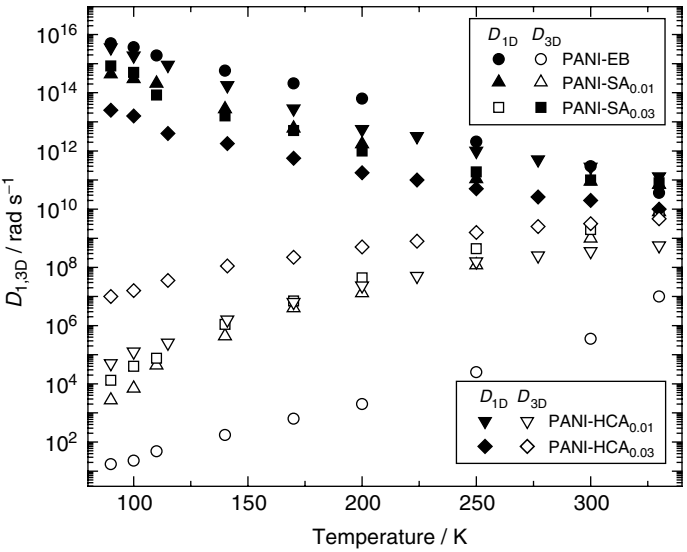

Fig. 10. Temperature dependence of effective coefficients for intrachain D_{1D} and interchain D_{3D} polaron diffusion in the PANI-EB and slightly SA- and HCA-doped PANI samples. [From Refs. 12(b), 44(b), and 45(a) with permission.]

also be considered in terms of the Kivelson formalism[64] of isoenergetic interchain charge transfer. Figure 11 shows that the experimental data for σ_{1D} of the initial PANI sample is well fitted by Eq. 12 with $n = 8.5$. This approach is not evident for PANI doped up to $0.01 \leq y \leq 0.03$, with a flatter temperature dependence. The model of charge-carrier scattering on optical phonons in metal-like domains seems to be more convenient for explaining the conductivity behavior.

As seen in Fig. 11, the $\sigma_{1D}(T)$ dependence, for example, the slightly doped PANI-SA, is also fairly well fitted by Eq. 15 with $\hbar\omega_{ph} \approx 0.1$ eV. This value lies near the energy (0.19 eV) of the polaron pinning in heavily doped PANI-ES.[72] The strong temperature dependence σ_{3D} of the initial sample can then be interpreted in the framework of the model of the activation charge transfer between the polymer chains described by Eq. 13, with E_a different for low- and high-temperature regions (Fig. 11). The respective interchain charge transfer in these polymers occurs with E_a=0.1 eV (Fig. 11).

Spin–lattice and spin–spin relaxation times measured by the saturation method at X-band ESR for the PANI-PTSA with $y = 0.5$ are $T_1 = 1.1 \times 10^{-7}$ s and $T_2 = 1.6 \times 10^{-8}$ s.[48] For polarons, diffusion along and between polymer chains in this highly doped polymer, $D_{1D} = 8.1 \times 10^{11}$ rad s^{-1} and $D_{3D} = 2.3 \times 10^{8}$ rad s^{-1}, should be evaluated from Eqs. 10. The value $D_{1D}/D_{3D} \approx 10^4$ substantially exceeds the value $D_{1D}/D_{3D} \approx 50$ obtained for highly doped PANI-HCA.[71] The corresponding terms of conductivity due to possible polaron mobility calculated from Eq. 12 are $\sigma_{1D} = 29$ S cm^{-1} and $\sigma_{3D} = 2.4 \times 10^{-3}$ S cm^{-1}.

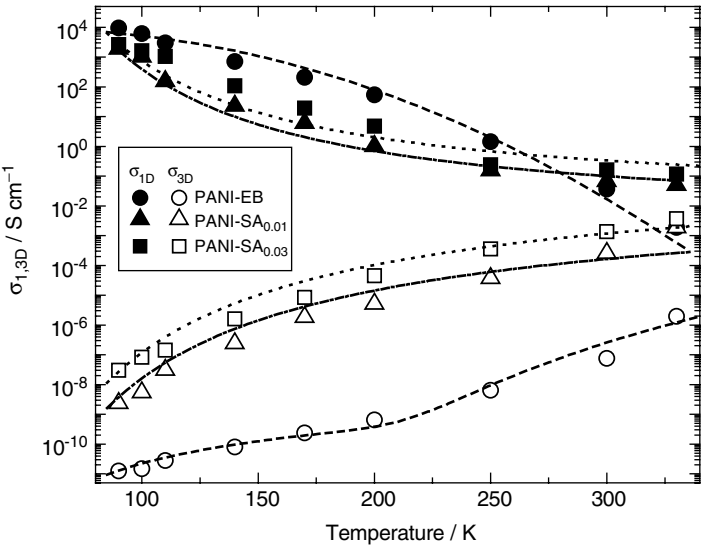

Fig. 11. Temperature dependence of the ac conductivity due to polaron motion along σ_{1D} and between σ_{3D} polymer chains in PANI-EB and slightly SA-doped PANI samples. The lines show the dependence calculated from Eq. 12 with $\sigma_0 = 4.5 \times 10^{-11}$ S K^{-1}s cm^{-1}, $k_1 = 3.1 \times 10^{12}$ s K$^{-9.5}$, and $n = 8.5$ (upper dashed line), from Eq. 15 with $\sigma_0 = 3.95 \times 10^{-6}$ S cm^{-1} K^{-1} and $\hbar\omega_{ph} = 0.12$ eV (upper dash–dotted line), $\sigma_0 = 1.75 \times 10^{-6}$ S cm^{-1} K^{-1} and $\hbar\omega_{ph} = 0.11$ eV (upper dotted line), and from Eq. 13 with $\sigma_0 = 8.2 \times 10^{-21}$ S K^{-1}s$^{0.8}$cm^{-1} and $E_a = 0.033$ eV (low-temperature region) and $\sigma_0 = 3.9 \times 10^{-12}$ S K^{-1}s$^{0.8}$cm^{-1} and $E_a = 0.41$ eV (high-temperature region) (lower dashed line), $\sigma_0 = 4.5 \times 10^{-14}$ S K^{-1}s$^{0.8}$cm^{-1} and $E_a = 0.10$ eV (lower dash–dotted line), $\sigma_0 = 3.1 \times 10^{-13}$ S K^{-1}s$^{0.8}$cm^{-1} and $E_a = 0.10$ eV (lower dotted line). [From Ref. 44(b) with permission.]

Note, however, that the steady-state saturation method used to obtain relaxation parameters of PC in lightly doped polymers reveals serious limitations for the study of spin dynamics in highly doped polymers, as seen below.

4. CHARGE TRANSFER IN HIGHLY DOPED CONDUCTIVE POLYMERS

The saturation of spin packets in highly doped polymers decreases significantly due to the increase in spin–spin and spin–lattice interactions. In the ESR spectra of such samples, the Dysonian term normally appears due to the formation of a skin layer with thickness δ. In contrast with the classic ESR signal, the Dyson-like spectrum shape "feels" both the spin polarons and the spinless bipolarons diffusing through a skin layer. It is possible to determine the intrinsic conductivity σ_{ac} of the sample directly from its Dysonian ESR spectrum. If the skin–layer is formed on the surface of a spherical powder particle with radius R, the coefficients A and D in Eq. 5 can be determined from Eqs. 16,[73]

$$\frac{4A}{9} = \frac{8}{p^4} - \frac{8\,(\sinh p + \sin p)}{p^3\,(\cosh p - \cos p)} + \frac{8 \sinh p \sin p}{p^2\,(\cosh p - \cos p)^2} + \frac{(\sinh p - \sin p)}{p\,(\cosh p - \cos p)} - \frac{(\sinh^2 p - \sin^2 p)}{(\cosh p - \cos p)^2} + 1 \tag{16a}$$

$$\frac{4D}{9} = \frac{8\,(\sinh p - \sin p)}{\mathrm{p}^3\,(\cosh p - \cos p)} - \frac{4\,(\sinh^2 p - \sin^2 p)}{\mathrm{p}^2\,(\cosh p - \cos p)^2} + \frac{(\sinh p + \sin p)}{p\,(\cosh p - \cos p)} - \frac{2\sinh p \sin p}{(\cosh p - \cos p)^2} \tag{16b}$$

where $p = 2R/\delta$, $\delta = \sqrt{2/\mu_0\omega_e\sigma_{ac}}$, and μ_0 is the magnetic permeability for vacuum.

Figure 12 exhibits the temperature dependence of the ac conductivity of some doped PANI samples determined from their Dysonian D-band ESR spectra using Eqs. 5 and 16. The shape of the temperature dependence demonstrates nonmonotonous temperature dependence with a characteristic point $T_c \approx 170$–200 K. Such a temperature dependence can be a result of two parallel processes: the above-mentioned tunneling of charge carriers at $T \leq T_c$ (the semiconducting regime), and their interaction with lattice phonons at $T \geq T_c$ (the metallic regime), as described by Eqs. 14 and 15, respectively.

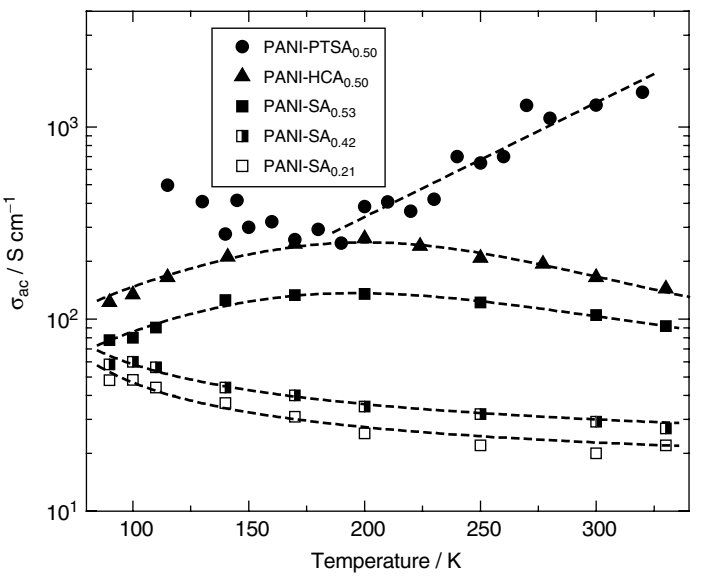

Fig. 12. Temperature dependence of ac conductivity determined from Dysonian ESR spectra of doped PANI-ES. Top to down dashed lines show the dependence calculated from Eq. 14 with $\sigma_0 = 24.9$ S (K cm)$^{-1}$ and from a combination of Eqs. 14 and 15 with, respectively, $\sigma_{0_1} = 1.47$ S cm^{-1} K^{-1}, $\sigma_{0_2} = 2.1 \times 10^{-2}$ S cm^{-1} K^{-1}, and $\hbar\omega_{ph} = 0.12$ eV; $\sigma_{0_1} = 0.86$ S cm^{-1} K^{-1}, $\sigma_{0_2} = 4.3 \times 10^{-2}$ S cm^{-1} K^{-1}, $\hbar\omega_{ph} = 0.087$ eV; $\sigma_{0_1} = 0.48$ S cm^{-1} K^{-1}, $\sigma_{0_2} = 8.5 \times 10^{-3}$ S cm^{-1} K^{-1}, $\hbar\omega_{ph} = 0.049$ eV; $\sigma_{0_1} = 0.41$ S cm^{-1} K^{-1}, $\sigma_{0_2} = 5.7 \times 10^{-3}$ S cm^{-1} K^{-1}, $\hbar\omega_{ph} = 0.052$ eV. [From Refs. 12(b), 44(b), and 45(a) with permission.]

Figure 12 shows that the experimental σ_{ac} values obtained for PANI are well fitted by a combination of Eqs. 14 and 15. The energy of lattice phonons $h\omega_{ph}$ determined for highly doped PANI-ES lies near (0.066 eV) evaluated from data obtained by Wang et al.[74] The constant of charge carrier diffusion along the chains of PANI-SA and PANI-HCA, $D_{1D} = \sigma_{ac}/e^2 n(\varepsilon_F) c_{1D}^2 = (0.5–1.1) \times 10^{14}$ rad s^{-1}, exceeds at least by an order of magnitude the D_{1D} determined above for slightly doped samples at room temperature. The mean free path was calculated for the highly doped PANI-ES to be 0.5–6 nm. This value is smaller than that estimated for oriented *trans*-PA,[69] but holds, however, for extended electron states in these polymers as well.

An intrinsic conductivity determined for the highly doped PANI-PTSA sample at $T \geq 170$ K is described by Eq. 15 with $h\omega_{ph} = 0.022$ eV (Fig. 12). The value calculated at 300 K, 1.3×10^3 S cm^{-1}, exceeds the σ_{1D} and σ_{3D} values assessed above, and indicates that the saturation method cannot be applied for the study of spin dynamics in highly doped polymers.

The conductivity of heavily doped PANI-SA, PANI-HCA, and PANI-PTSA estimated from their Dysonian ESR spectra is much smaller than that of $\approx 10^7$ S cm^{-1} calculated theoretically;[75,76] however, it is near that obtained for metal-like domains in PANI-ES at 6.5 GHz.[76]

The data obtained allows us to conclude that highly doped PANI-SA and PANI-HCA are Fermi glasses with electronic states localizes at the Fermi energy due to disorder, whereas PANI-TPSA and PANI-CSA are disordered metals on the metal–insulator boundary, so that the metallic quality of the emeraldine form of PANI grows in the series PANI-HCA → PANI-SA → PANI-PTSA → PANI-CSA.

5. HIGH–FIELD SATURATION TRANSFER ESR METHOD IN THE STUDY OF CONDUCTIVE POLYMERS

An additional advantage of D-band ESR is that it offers the opportunity to investigate the macromolecular mobility in conductive polymers with PC interacting with heteroatoms and, therefore, possessing anisotropic magnetic parameters. Such motion is *a priori* realized with correlation times in the range of $10^{-3} > \tau_c > 10^{-7}$ s.[77] The most sensitive to such molecular motions are the $\pi/2$-out-of-phase first term of the first harmonic of dispersion and second harmonic of absorption spectra. According to the saturation-transfer ESR (ST–ESR) method,[79] if all radicals rotate about their own *x*-axis, the conditions of adiabatic saturation are fulfilled for some of the radicals oriented by the *x*-axis along the external magnetic field B_0 and cannot be realized for radicals with other orientations. This results in the elimination of the saturation for radicals whose *y* and *z* axes are oriented parallel to the field B_0 and in the decrease of their contribution to the total ST–ESR spectrum.

It was demonstrated[11,12,78] that all terms of anisotropic magnetic parameters of stable organic radicals are registered separately at D-band ESR. In contrast with the nitroxide radical usually used as a spin probe or label in condensed systems, the native polaron with anisotropic magnetic parameters becomes itself a stable spin label. Therefore, the nearest environment of such PC remains undisturbed and the results

obtained on structure or spin and molecular motion become more accurate and complete. Besides, the sensitivity of the method increases with ω_e,[79,80] so it can be used more efficiently in the study of macromolecular dynamics in conductive polymers at D-band ESR. By measuring ESR at this frequency, where both dispersion terms of PC are localized on the polymer chain, it is possible to determine separately the relaxation times (see above) and the correlation time of anisotropic activation motion with a chain near, for example, the main molecular x-axis from the following simple equation,[12]

$$\tau_c^x = \tau_{c0}^x \left(u_3^x / u_3^y \right)^{\alpha} = \tau_{c0}^x \exp\left(\frac{E_a}{k_B T} \right) \tag{17}$$

where α is a constant determined by an anisotropy of the g-factor and E_a is an activation energy of the radical motion near a specific molecular axis. The preexponential factor τ_{c0}^x is the lowest limit for the correlation times in a respective polymer matrix.

From Fig. 4, it is seen how the relative intensity of the $\pi/2$-out-of-phase term of D-band ESR dispersion spectra of P3OT changes with temperature. The increase of the spectral X-component u_3^x with increasing temperature shows the appearance of such

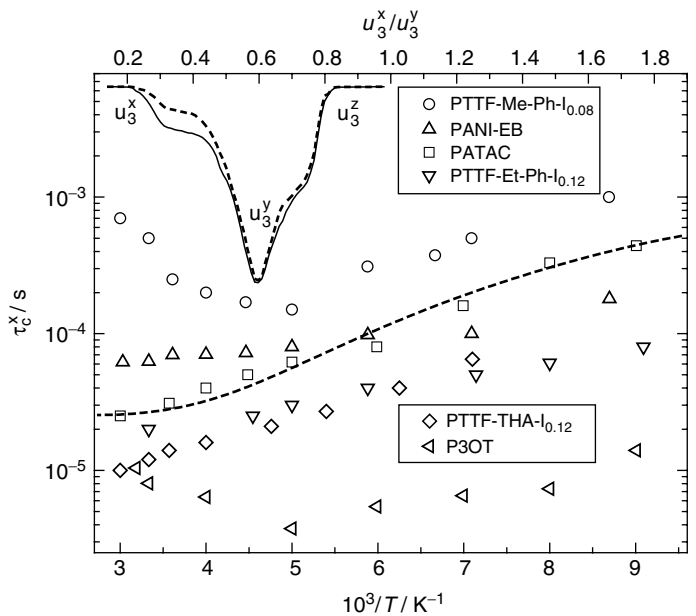

Fig. 13. Arrhenius dependence of correlation times for superslow librations near the polymer main x-axis of polarons R_1 localized on polymer chain segments in some conductive polymers evaluated from their ST–ESR spectra (inset). In the inset, the typical $\pi/2$-out-of-phase dispersion spectra registered at 100 K (solid line) and 200 K (dashed line) are shown. The dependence calculated from Eq. 17 is shown by a dotted line. [From Refs. 12(b), 21(b), 24, 30(b), and 45(a) with permission.]

saturation transfer over the spectrum due to superslow macromolecular libration dynamics. The Arrhenius dependence of τ_c^x determined from Eq. 17 for such motion in different conductive polymers is presented in Fig.13.

The value deduced for P3OT decreases with a temperature increase up to $T_c \approx 150$ K and then increases above this critical temperature. Note that Masubuchi et al.[81] observed the proton nuclear magnetic resonance (^{1}H NMR) T_1 temperature dependence with the same critical temperature. This result was attributed to the motion of the alkyl chain end groups. The dependences obtained can be interpreted in the frame of the superslow 1D libration of the polymer chains together with polarons near their main x-axis at low temperatures for $T \leq T_c$, whereas their high-temperature part can be explained by the collective 2D motion at $T \geq T_c$ with $E_a = 0.069$ eV. Treatment of this polymer by annealing and by both recrystallization and annealing leads to lower (0.054 eV) and higher (0.073 eV) E_a values, respectively.[30]

The energy of activation also depends on the structure and the doping level of a polymer. For example, the values obtained for PANI–EB, laser-modified PATAC, iodine doped PTTF-Me-Ph, PTTF-Et-Ph, and PTTF–THA from the data summarized in Fig. 13 and Eq. 17 are 0.015, 0.043, 0.036, 0.021, and 0.041 eV, respectively. Slight doping of an initial PTTF sample doubles the activation energy of macromolecular librations. The E_a values obtained at D-band ESR are comparable with those determined for interchain charge transfer in doped PTTF at a lower measuring frequency,[26] indicating the interaction of pinned and mobile polarons in this polymer matrix. The upper limit for the correlation time registered by the ST–ESR method is 4×10^{-4} s at 66 K for P3OT and 1×10^{-4} s for PTTF-Me-Ph and PANI-EB at 75 and 125 K, respectively.

6. HIGH-FIELD SPIN PROBE METHOD IN THE STUDY OF CONDUCTIVE POLYMERS

In some conductive polymers, pairs of polarons can merge into spinless bipolarons.[8] In this case, the method of spin–label and probe,[82,83] especially at D-band ESR,[11] seems to be more effective for the study of their structure and dynamics.

The X- and D-band absorption ESR spectra of a nitroxide radical, 2,2,6,6-tetramethyl-1-oxypiperid-4-yl acetic acid, introduced as both a probe and dopant in PP and as a probe in a frozen nonpolar model system, are shown in Fig. 14.[84] The X-band ESR single line of PC (R) stabilized in PP overlaps the lines of nitroxide radical rotating with correlation time $\tau_c > 10^{-7}$ s^{-1}.

The D-band ESR spectra of these model and modified polymer systems are more informative (Fig. 14). At this waveband, all terms of g- and A-tensors of the probe are completely resolved. Nevertheless, the asymmetric spectrum of radicals R stabilized in PP with magnetic parameters $g_{\parallel}^R = 2.00380$, $g_{\perp}^R = 2.00235$, and $\Delta B_{pp} = 5.7$ G is registered near the z component of the probe spectrum. In nonpolar toluene, the probe is characterized by $g_x = 2.00987$, $g_y = 2.00637$, g_z=2.00233, $A_x = A_y = 6.0$ G, and $A_z = 33.1$ G. The difference $\Delta g^R = 1.45 \times 10^{-3}$ corresponds to an excited electron configuration in R with $\Delta E_{\sigma\pi^*} = 5.1$ eV. In conducting PP, the g_x value of the probe decreases to 2.00906 and its x- and y-components become broadened by 40 G (Fig. 14). In addition, the shape of the probe spectrum shows the localization of PC

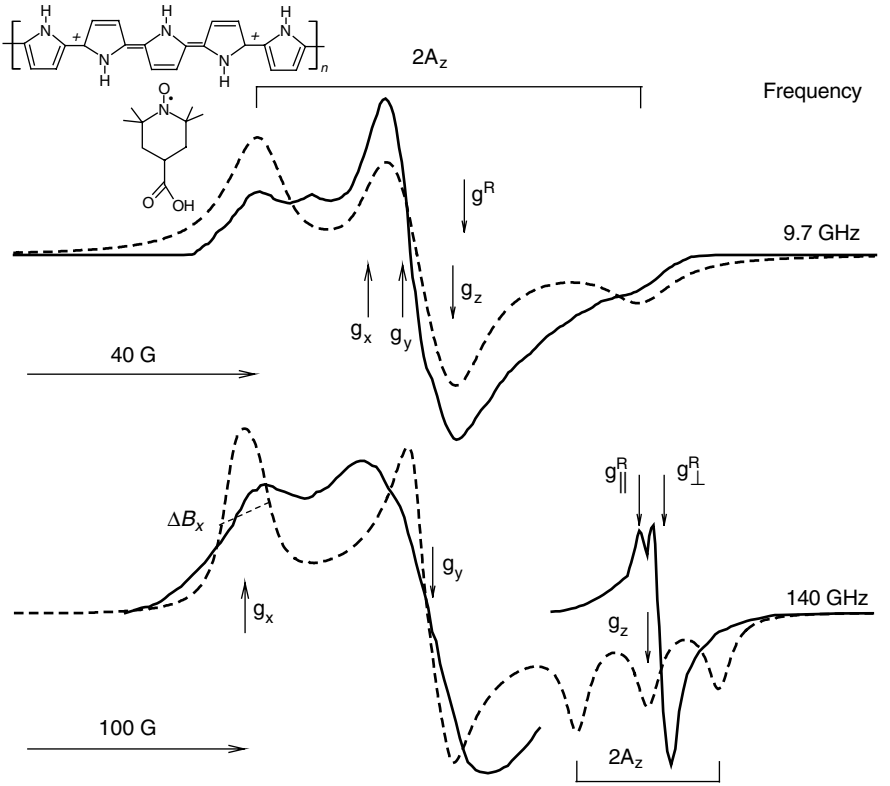

Fig. 14. Both X- and D-band ESR absorption spectra of a nitroxide radical in frozen (120 K) toluene as a spin probe (dotted line) and in conductive PP (solid line) as a dopant and spin probe. The anisotropic spectrum of localized PC marked by the symbol *R* and measured at a smaller amplification is also shown in the lower spectrum. The bipolaron spreads out over a larger number of units than shown schematically in this figure. [From Refs. 12(b) and 84 with permission.]

R in the polymer pocket of 1 nm-size, that is, the charge in this polymer is really transferred by spinless bipolarons.

The fragments with a considerable dipole moment are *a priori* absent in an initial PP. Besides, the dipole–dipole interactions between the radicals can be neglected due to a low concentration of the probe and PC localized on the chain. Therefore, the change in the probe's magnetic resonance parameters may be caused by a Coulombic interaction of the probe active fragment with mobile spinless bipolarons. The effective electric dipole moment of bipolarons diffusing near the probe was determined from the shift of the g_x component to be μ_v=2.3 D. The shift of g_x may be calculated based on the electrostatic interaction of the probe and bipolaron dipole by using the potential of the electric field induced by the bipolaron near the probe site,[84,85]

$$\Delta g_x = \frac{6.10^{-3} e r_{NO} k_B T}{I \mu_u} (x \coth x - 1) \qquad (18)$$

where r_{NO} is the distance between N and O atoms in the probe active fragment, I is the resonant overlapping integral of the C=C bond, μ_u is the dipole moment of the probe, $x = 2\mu_u\mu_v(\pi\varepsilon\varepsilon_0 k_B T r^3)^{-1}$, ε and ε_0 are the dielectric constants for PP and vacuum, respectively, r is the distance between the nitroxide radical and the bipolaron. The value of $r = 0.92$ nm is obtained by using $\mu_u = 2.7$ D,[86] $\mu_v = 2.3$ D, and $r_{NO} = 0.13$ nm.[49]

The effective spin–spin relaxation rate $T_2^{-1} = T_{2(0)}^{-1} + T_{2(D)}^{-1}$ is defined by relaxation of radicals not interacting with the environment, $T_{2(0)}^{-1}$, and the increment due to dipole–dipole interactions, $T_{2(D)}^{-1} = \gamma_e\delta(\Delta B_{pp}^{x,y})$. The characteristic time τ_c of such an interaction was calculated from the broadening of the spectral lines using Eq. 10b with $J(\omega_e) = 2\tau_c/(1 + \omega_e^2\tau_c^2)$ to be $\tau_c = 8.1 \times 10^{-11}$ s. The value is close to the time of polaron hopping between chains, $\tau_{3D} \cong 1.1 \times 10^{-10}$ s estimated for slightly doped PP.[87] Taking into account that the average time between the translating jumps of charge carriers is defined by the diffusion coefficient D and by the average jump distance equal to a product of lattice constant c_{1D} on the half-width of the bipolaron $N_{bp}/2$, $\tau_c = 1.5\langle c_{1D}^2 N_{bp}^2\rangle/D$, and by using $D = 5 \times 10^{-3}$ cm^2 s^{-1} typical for conductive polymers, it is possible to determine $\langle c_{1D}N_{bp}\rangle = 3$ nm, equal approximately to four pyrrole rings.

By measuring at D-band, all anisotropic magnetic parameters of organic PC allows us to determine the subtle features of structure, conformation, dynamics, and polarity of the PC microenvironment in different condensed systems.[11,12,78] At this waveband, the correlation times of radical rotation near the main axis can be defined separately from the broadening of corresponding spectral components $\delta(\Delta B_i)$. Krinichnyi et al.[88] showed that the method of spin macroprobe can be used for more detailed investigations of the polymer systems in solution. The method is based on the analysis of simultaneous rotation in the system under study of both the nitroxide radical as a spin microprobe and a single microcrystal of a suitable ion-radical salt as a spin macroprobe. The macroprobe tends to orient the main crystal axis along the direction B_0 to attain the minimum energy of spin interaction with the magnetic field. Such a reorientation process is easily registered by its ESR line shift to lower magnetic fields.

The inset in Fig. 15 shows a D-band ESR spectrum of a frozen nujol/*tert*-butylbenzene mixture in whom a nitroxide radical is solved as a spin microprobe and a dibenzotetrathiafulvalene$_3$PtBr$_6$, (DBTTF$_3$PtBr$_6$) single microcrystal with the characteristic size of $\approx 10^{-4}$ mm^3 is introduced as a spin macroprobe. The change in the nitroxide radical spectrum shape below the T_g of the matrix glass transition is caused by its Brownian diffusion rotation. The correlation time $\tau_c = 1/\gamma_e\delta(\Delta B_i)$ of the spin microprobe reorientation was determined [78] to be $4.7\times10^{-20}\exp(0.57\text{ eV}/k_BT)$ s. The spin macroprobe was preliminary oriented by its d crystallographic axis along the magnetic field at a temperature significantly exceeding T_g. Then, the spin-modified sample is frozen down to $T \leq T_g$, turned by 90^0 (upper spectrum in the inset), and slowly warmed to $T \cong T_g$. The ESR line of the spin macroprobe is shifted from an initial position $B(t = 0)$ at $t = 0$ to a lower magnetic field $B(t)$, as shown on the lower spectrum in the inset. This line shift follows an exponential law, and attains the maximal value, $\delta B \approx 200$ G for this sample at $t \to \infty$ (Fig. 15).

The dynamics of the spin macroprobe depends on many parameters of the matrix and can be described by the differential equation for a one-point-fixed oscillator

$$\dot{\varphi} + \tau_m^{-1}\varphi = 0 \tag{19}$$

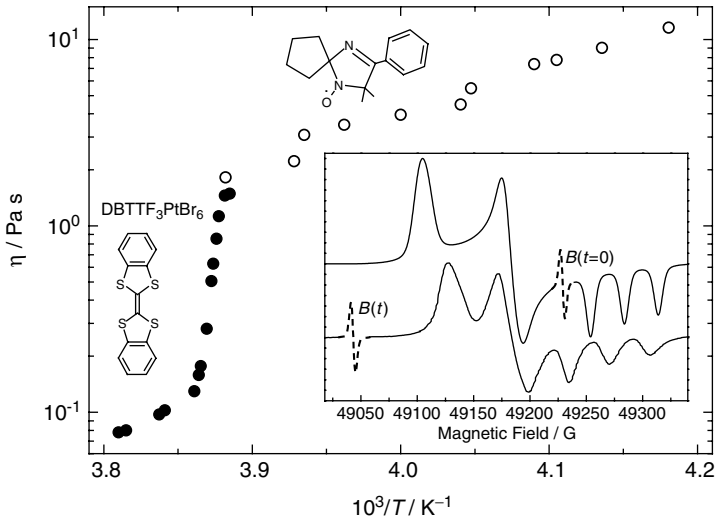

Fig. 15. The Arrhenius dependence of the dynamic viscosity η in the mixture obtained by both spin microprobe (open symbols) and spin macroprobe (filled symbols) methods. Inset: D-band ESR spectra of nitroxide radical (solid line) and single-crystal $DBTTF_3PtBr_6$ (dashed lines) introduced into a frozen and heat softened nujol/*tert*-butylbenzene mixture (1:10) at t = 0 (upper spectrum) and arbitrary t at $T \leq T_g$ (lower spectrum) time period. (From Ref. 89 with permission.]

where $\varphi(t) = \arccos[\delta B(t)/\delta B(t\rightarrow\infty)] = \varphi_0 \exp(-t/\tau_m)$, $\tau_m = 6\pi\eta r^3/(NV\mu_O\mu_B B_0)$ is the mechanical relaxation time, η is the coefficient of dynamic viscosity of the matrix, r and V are the characteristic size and volume of the crystal, respectively, and N is the PC bulk concentration. This allows us to determine the dynamic viscosity of the system under consideration, by using the Stokes equation:

$$\eta(\mathrm{T}) = \frac{3k_B T}{4\pi r^3}\,\tau_c \tag{20}$$

Figure 15 depicts the temperature dependence of the viscosity of the model system, defined by the spin micro- and macroprobe methods. As expected, $\eta(T) \propto T\exp(E_a/k_B T)$ at $T_g \approx 256$ K. At these temperatures, a spin probe reflects the motion of the radical glass-like microenvironment. The change in viscosity seems to have an activation character at $T \geq T_g$.

7. CONCLUDING REMARKS

The data presented in this chapter show the variety of electronic processes that take place in the low-dimensional organic conductive polymers, caused by the structure, conformation, packing, and degree of ordering of polymer chains, and also by the amount and type of the dopant introduced into the polymer matrix. The most important deductions are the following.

Spin and spinless nonlinear excitations exist as charge carriers in organic conductive polymers. The number of these carriers depends on the various properties of the polymer and the dopant introduced. With increasing doping level some polaron pairs merge into diamagnetic bipolarons. However, such a process can be restricted in some polymers due to their structural–conformational peculiarities. The doping of a polymer initiates changes in the charge-transfer mechanism. Conductivity in neutral or weakly doped samples is defined mainly by isoenergetic charge tunneling, which is characterized by a high interaction of spins with several phonons of a lattice and leads to the correlation of Q1D spin motion and interchain charge transfer. This mechanism ceases to dominate with the increase of doping level, and the charge can be transferred by its thermal activation from widely separated localized states in the gap to close localized states in the tails of the valence and conducting bands. Therefore, complex quasiparticles, namely, the molecular-lattice polarons, are formed in some polymers due to libron–phonon interactions analogous to that in organic molecular crystals. Note that as conductive polymers have *a priori* a lower dimensionality compared to molecular crystals, the dynamics of charge carriers is more anisotropic. In heavily doped samples, the dominant mechanism is the interchain charge transport, characterized by a strong interaction of charge carriers with lattice phonons.

The higher spectral resolution at D-band provides a higher accuracy of all magnetic measured magnetic parameters, with the g-factor of organic free radicals an important informative characteristic. As in the case of other organic solids, this allows us to establish the correlation between the structure of organic radicals and their g-tensor principal values, and to identify the PC in conductive polymers. High-field ESR allows us to obtain qualitatively new information on the spin carrier and on molecular dynamics, as well as on the magnetic and relaxation properties of polymer systems. Further progress in the study of conductive polymers is the use of different pulse methods at D-band ESR, for example, light-induced ESR (LESR) and spin–echo. Such studies are currently in progress in our laboratory.

ACKNOWLEDGMENTS

Support by the Russian Foundation of Basic Research, grants 97-03-33707, 01-03-33255, 03-03-04005, 05-03-33148, by the UK Royal Society, grant 638072.P885/bll, and by the German Foundation Deutsche Forschungsgemeinschaft (DFG), grant 436 RUS 113/734/1-1, is gratefully acknowledged. The author expresses his gratitude to E. Fanghänel for the gift of polytetrathiafulvalenes, to G. Hinrichsen, A.P. Monkman and B. Wessling for the gift of polyanilines, to S.D. Chemerisov and N.N. Denisov for assistance in the ESR experiments, and to S.A. Brazovskii, H.-K. Roth, K. Lüders, and Y.S. Lebedev for fruitful discussions.

REFERENCES

1. (a) *Encyclopedia of Polymeric Materials*, Salamone, J.C., Ed.; CRC Press: Boca Raton, Fl., 1996. (b) *Handbook of Organic Conductive Molecules and Polymers*, Nalwa, H.S., Ed.; John Wiley & Sons, Inc.: Chichester, New York, 1997; Vols. 1–4.

2. (a) *Handbook of Conducting Polymers*, Scotheim, T.E.; Elsenbaumer, R.L.; Reynolds, J.R., Eds.; Marcel Dekker: New York, 1997. (b) *Handbook of Conducting Polymers*, Skotheim, T.; Elsenbaumer, R.; Reynolds, J., Eds.; Marcel Dekker, Inc., 1998. (c) *Conducting Polymers, Fundamentals and Applications: A Practical Approach*, Chandrasekhar, P., Ed.; Kluwer Academic Publishers: Boston, MA, 1999. (d) *Encyclopedia of Polymer Science and Technology, Part 3*, Mark, H.F., Ed.; Wiley-Interscience: New York, 2004. (e) *One-Dimensional Metals: Conducting Polymers, Organic Crystals, Carbon Nanotubes*, Roth, S.; Carroll, D., Eds.; Wiley-VCH: Weinheim, 2004.
3. Peierls, R.E. *Quantum Theory of Solids*, Oxford University Press: London, 1955.
4. Su, W.P.; Schrieffer, J.R.; Heeger, A.J. *Phys. Rev. B* **1980,** *22*, 2209.
5. Brédas, J.L. In *Handbook of Conducting Polymers*, Scotheim, T.E., Ed.; Marcel Dekker, Inc.: New York, 1986; Vol. 2, Chapt. 25, pp. 859–913.
6. Chance, R.R.; Boudreaux, D.S.; Brédas, J.L.; Silbey, R. In *Handbook of Conducting Polymers*, Scotheim, T.E., Ed.; Marcel Dekker, Inc.: New York, 1986; Vol. 2, Chapt. 24, pp. 825–857.
7. Devreux, F.; Genoud, F.; Nechtschein, M.; Villeret, B. In *Electronic Properties of Conjugated Polymers*, Kuzmany, H.; Mehring, M.; Roth, S., Eds.; Springer-Verlag: Berlin, 1987; Vol. 76, pp. 270–276.
8. (a) Bernier, P. In *Handbook of Conducting Polymers*, Scotheim, T.E., Ed.; Marcel Deccer, Inc.: New York, 1986; Vol. 2, Chapt. 30, pp. 1099–1125. (b) Mizoguchi, K.; Kuroda, S. In *Handbook of Organic Conductive Molecules and Polymers,* Nalwa, H.S., Ed.; John Wiley & Sons, Inc.: Chichester, New York, 1997; Vol. 3, Chapt. 6, pp. 251–317.
9. (a) Thomann, H.; Dalton, L.R. In *Handbook of Conducting Polymers,* Scotheim, T.E., Ed.; Marcel Dekker, Inc.: New York, 1986; Vol. 2, Chapt. 32, pp. 1157–1190. (b) Clarke, T.C.; Scott, J.C. In *Handbook of Conducting Polymers,* Skotheim, T.A., Ed.; Marcel Dekker, Inc.: New York, 1986; Vol. 2, Chapt. 31, pp. 1127–1156.
10. Altshuler, S.A.; Kozirev, B.M. *Electron Paramagnetic Resonance* (Russ), Fizmatgiz: Moscow, 1961.
11. (a) Krinichnyi, V.I. *J. Biochem. Biophys. Meths.* **1991,** *23*, 1. (b) Krinichnyi, V.I. *Appl. Magn. Reson.* **1991,** *2*, 29, and references cited therein.
12. (a) Krinichnyi, V.I. *2-mm Wave Band EPR Spectroscopy of Condensed Systems*, CRC Press: Boca Raton, FL, 1995. (b) Krinichnyi, V.I. *Synth. Met.* **2000,** *108*, 173. See also website: http://hf-epr.sitesled.com/publications.htm
13. Poole, C.P. *Electron Spin Resonance*, International Science Publishers: London, 1967.
14. Altshuler, S.A.; Kozirev, B.M. *Electron Paramagnetic Resonance of Compounds of Elements of Intermediate Groups* (Russ), 2 ed.; Nauka: Moscow, 1972.
15. (a) Krinichnyi, V.I. *Russ. Chem. Rev.* **1996,** *65*, 81. (b) Krinichnyi, V.I. *Russ. Chem. Rev.* **1996,** *65*, 521. (c) Krinichnyi, V.I. *Phys. Solid State* **1997,** *39*, 1.
16. Chien, J.C.W. *Polyacetylene: Chemistry, Physics and Material Science*, Academic Press: Orlando, FL, 1984.
17. Krinichnyi, V.I.; Tkachenko, L.I.; Kozub, G.I. *Khimich. Fiz.* **1989,** *8*, 1282.
18. (a) Krinichnyi, V.I.; Pelekh, A.E.; Brezgunov, A.Y.; Tkachenko, L.I.; Kozub, G.I. *Mater. Sci. Eng.* **1991,** *17*, 25. (b) Pelekh, A.E.; Krinichnyi, V.I.; Brezgunov, A.Y. ; Tkachenko, L.I.; Kozub, G.I. *Vysokomol. Soedin. A* **1991,** *33*, 1731.
19. Krinichnyi, V.I.; Pelekh, A.E.; Lebedev, Y.S.; Tkachenko, L.I.; Kozub, G.I.; Barra, A.L.; Brunel, L.C.; Robert, J.B. *Appl. Magn. Reson.* **1994,** *7*, 459.

20. Goldberg, I.B.; Crowe, H.R.; Newman, P.R.; Heeger, A.J.; MacDiarmid, A.G. *J. Chem. Phys.* **1979,** *70*, 1132.
21. (a) Roth, H.-K.; Krinichnyi, V.I.; Schrödner, M.; Stohn, R.-I. *Synth. Met.* **1999,** *101*, 832. (b) Krinichnyi, V.I.; Roth, H.-K.; Schrödner, M. *Appl. Magn. Reson.* **2002,** *23*, 1.
22. Carrington, F.; McLachlan, A.D. *Introduction to Magnetic Resonance with Application to Chemistry and Chemical Physics*, Harper & Row: New York, 1967.
23. Traven, V.F. *Electronic Structure and Properties of Organic Molecules (Russ)*, Khimija: Moscow, 1989.
24. (a) Krinichnyi, V.I.; Pelekh, A.E.; Roth, H.-K.; Lüders, K. *Appl. Magn. Reson.* **1993,** *4*, 345. (b) Krinichnyi, V.I.; Denisov, N.N.; Roth, H.-K.; Fanghänel, E.; Lüders, K. *Polym. Sci. A* **1998,** *40*, 1259.
25. Roth, H.-K.; Krinichnyi, V.I. *Makromolec. Chem. Macromolec. Symp.* **1993,** *72*, 143.
26. (a) Roth, H.-K.; Gruber, H.; Fanghänel, E.; Trinh, V.Q. *Progr. Colloid Polym. Sci.* **1988,** *78*, 75. (b) Roth, H.-K.; Brunner, W.; Volkel, G.; Schrödner, M.; Gruber, H. *Makromolec. Chem. Macromolec. Symp.* **1990,** *34*, 293.
27. Nechtschein, M. In *Handbook of Conducting Polymers*, Skotheim, T.A.; Elsenbaumer, R.L.; Reynolds, J.R., Eds.; Marcel Dekker: New York, 1997; Chapt. 5, pp. 141–163.
28. *Thiophene and its Derivatives*, Gronowitz, S., Ed.; John Wiley & Sons, Inc.: New York, 1991.
29. Krinichnyi, V.I.; Grinberg, O.Y.; Nazarova, I.B.; Kozub, G.I.; Tkachenko, L.I.; Khidekel, M.L.; Lebedev, Y.S. *Bull. Acad. Sci. USSR, Div. Chem.* **1985,** *34*, 425.
30 (a) Roth, H.-K.; Krinichnyi, V.I. *Synth. Met.* **2003,** *137*, 1431. (b) Krinichnyi, V.I.; Roth, H.-K. *Appl. Magn. Reson.* **2004,** *26*, 395. (c) Krinichnyi, V.I.; Roth, H.-K.; Konkin, A.L. *Physica B* **2004,** *344*, 430.
31. Owens, J. *Phys. Stat. Solidi B* **1977,** *79*, 623.
32. Houze, E.; Nechtschein, M. *Phys. Rev. B* **1996,** *53*, 14309.
33. Molin, Y.N.; Salikhov, K.M.; Zamaraev, K.I. *Spin Exchange*, Springer: Berlin, 1980.
34. Patzsch, J. Ph.D. Dissertation, Technische Hochschule Leipzig, 1991.
35. Elliott, R.J. *Phys. Rev.* **1954,** *96*, 266.
36. Williams, J.M.; Ferraro, J.R.; Thorn, R.J.; Carlson, K.D.; Geiser, U.; Wang, H.H.; Kini, A.M.; Whangboo, M.-H. *Organic Superconductors (Including Fullerenes): Synthesis, Structure, Properties, and Theory*, Prentice-Hall, Inc., Englewood Cliffs: NJ, 1992.
37. Trivedi, D.C. In *Handbook of Organic Conductive Molecules and Polymers*, Nalwa, H. S., Ed.; John Wiley & Sons, Inc.: Chichester, 1997; Vol. 2, Chapt. 12, pp. 505–572.
38. Ginder, J.M.; Richter, A.F.; MacDiarmid, A.G.; Epstein, A.J. *Solid State Commun.* **1987,** *63*, 97.
39. Epstein, A.J.; MacDiarmid, A.G. *J. Molec. Electr.* **1988,** *4*, 161.
40. (a) Zuo, F.; Angelopoulos, M.; MacDiarmid, A.G.; Epstein, A.J. *Phys. Rev. B* **1987,** *36*, 3475. (b) MacDiarmid, A.G.; Epstein, A.J. *Faraday Disc.* **1989,** *88*, 317. (c) Epstein, A.J.; MacDiarmid, A.G. *Synth. Met.* **1991,** *41*, 601.
41. Stafstrom, S.; Brédas, J.L.; Epstein, A.J.; Woo, H.S.; Tanner, D.B.; Huang, W.S.; MacDiarmid, A.G. *Phys. Rev. Lett.* **1987,** *59*, 1464.
42. Saprigin, A.V.; Brenneman, K.R.; Lee, W.P.; Long, S.M.; Kohlman, R.S.; Epstein, A.J. *Synth. Met.* **1999,** *100*, 55.
43. Lubentsov, B.Z.; Timofeeva, O.N.; Saratovskikh, S.L.; Krinichnyi, V.I.; Pelekh, A.E.; Dmitrenko, V.V.; Khidekel, M.L. *Synth. Met.* **1992,** *47*, 187.

44. (a) Lux, F.; Hinrichsen, G.; Krinichnyi, V.I.; Nazarova, I.B.; Chemerisov, S.D.; Pohl, M. *Synth. Met.* **1993,** *55*, 347. (b) Krinichnyi, V.I.; Roth, H.-K.; Hinrichsen, G.; Lux, F.; Lüders, K. *Phys. Rev. B* **2002,** *65*, 155205. (c) Krinichnyi, V.I.; Roth, H.-K.; Hinrichsen, G. *Synth. Met.* **2003,** *135–136*, 431.
45. (a) Krinichnyi, V.I.; Chemerisov, S.D.; Lebedev, Y.S. *Phys. Rev. B* **1997,** *55*, 16233. (b) Krinichnyi, V.I.; Chemerisov, S.D.; Lebedev, Y.S. *Synth. Met.* **1997,** *84*, 819.
46. Krinichnyi, V.I. *Russ. Chem. Bull.* **2000,** *49*, 207.
47. (a) Krinichnyi, V.I.; Konkin, A.L.; Devasagayam, P.; Monkman, A.P. *Synth. Met.* **2001,** *119*, 281. (b) Konkin, A.L.; Shtyrlin, V.G.; Garipov, R.R.; Aganov, A.V.; Zakharov, A.V.; Krinichnyi, V.I.; Adams, P.N.; Monkman, A.P.; *Phys. Rev. B* **2002,** *66*, 075203.
48. (a) Krinichnyi, V.I.; Tokarev, S.V.; Roth, H.-K.; Schrödner, M.; Wessling, B. *Synth. Met.* **2005,** *152*, 165. (b) Krinichnyi, V.I.; Tokarev, S.V. *Polym. Sci. A* **2005,** *47*, 261.
49. Buchachenko, A.L.; Vasserman, A.M. *Stable Radicals (Russ)*, Khimija: Moscow, 1973.
50. Long, S.M.; Cromack, K.R.; Epstein, A.J.; Sun, Y.; MacDiarmid, A.G. *Synth. Met.* **1994,** *62*, 287.
51. (a) Goldenberg, L.M.; Pelekh, A.E.; Krinichnyi, V.I.; Roshchupkina, O.S.; Zueva, A.F.; Lyubovskaja, R.N.; Efimiv, O.N. *Synth. Met.* **1990,** *36*, 217. (b) Goldenberg, L.M.; Pelekh, A.E.; Krinichnyi, V.I.; Roshchupkina, O.S.; Zueva, A.F.; Lyubovskaja, R.N.; Efimiv, O.N. *Synth. Met.* **1991,** *43*, 3071.
52. Dyson, F.J. *Phys. Rev. B* **1955,** *98*, 349.
53. Vonsovskii, S.V. *Magnetism* (Russ), Nauka: Moscow, 1971.
54. Iida, M.; Asaji, T.; Inoue, M.B.; Inoue, M. *Synth. Met.* **1993,** *55*, 607.
55. (a) Kahol, P.K.; Pinto, N.J.; McCormick, B.J. *Solid State Commun.* **1994,** *91*, 21. (b) Lee, K.; Heeger, A.J.; Cao, Y. *Synth. Met.* **1995,** *69*, 261.
56. Blakemore, J.S. *Solid State Physics*, Cambridge University Press: Cambridge, 1985.
57. Lee, K.H.; Heeger, A.J.; Cao, Y. *Phys. Rev. B* **1993,** *48*, 14884.
58. Gullis, P.R. *J. Magn. Reson.* **1976,** *21*, 397.
59. Pelekh, A.E.; Krinichnyi, V.I.; Brezgunov, A.Y.; Tkachenko, L.I.; Kozub, G.I. *Vysokomolekul. Soedin. A* **1991,** *33*, 1731.
60. Abragam, A. *The Principles of Nuclear Magnetism*, Clarendon Press: Oxford, 1961.
61. Krinichnyi, V.I.; Pelekh, A.E.; Tkachenko, L.I.; Kozub, G.I. *Synth. Met.* **1992,** *46*, 13.
62. Nechtschein, M.; Devreux, F.; Genoud, F.; Guglielmi, M.; Holczer, K. *Phys. Rev. B* **1983,** *27*, 61.
63. Krinichnyi, V.I.; Pelekh, A.E.; Tkachenko, L.I.; Kozub, G.I. *Synth. Met.* **1992,** *46*, 1.
64. Kivelson, S. *Phys. Rev. B* **1982,** *25* , 3798.
65. Epstein, A.J. In *Handbook of Conducting Polymers*, Scotheim, T.E., Ed.; Marcel Dekker: New York, 1986; Vol. 2, Chapt. 29, pp. 1041–1097.
66. Parneix, J.P.; El Kadiri, M. In *Electronic Properties of Conjugated Polymers*, Kuzmany, H.; Mehring, M.; Roth, S., Eds.; Springer-Verlag: Berlin, 1987; Vol. 76, pp. 23–26.
67. Long, A.R. *Adv. Phys.* **1982,** *31*, 553.
68. Mott, N.F.; Davis, E. A. *Electronic Processes in Non-Crystalline Materials*, Clarendon Press: Oxford, 1979.
69. Kivelson, S.; Heeger, A.J. *Synth. Met.* **1988,** *22*, 371.
70. Kunugi, Y.; Harima, Y.; Yamashita, K.; Ohta, N.; Ito, S. *J. Mater. Chem.* **2000,** *10*, 2673.

71. Mizoguchi, K.; Nechtschein, M.; Travers, J.-P.; Menardo, C. *Phys. Rev. Lett.* **1989,** *63*, 66.
72. Javadi, H.H.S.; Cromack, K.R.; MacDiarmid, A.G.; Epstein, A.J. *Phys. Rev. B* **1989,** *39*, 3579.
73. Chapman, A.C.; Rhodes, P.; Seymour, E.F.W. *Proc. Phys. Soc.* **1957,** *B 70*, 345.
74. (a) Wang, Z.H.; Li, C.; Scherr, E.M.; MacDiarmid, A.G.; Epstein, A.J. *Phys. Rev. Lett.* **1991,** *66*, 1745. (b) Wang, Z.H.; Scherr, E.M.; MacDiarmid, A.G.; Epstein, A.J. *Phys. Rev. B* **1992,** *45*, 4190.
75. Lim, H.Y.; Jeong, S.K.; Suh, J.S.; Oh, E.J.; Park, Y.W.; Ryu, K.S.; Yo, C.H. *Synth. Met.* **1995,** *70*, 1463.
76. Joo, J.; Oh, E. J.; Min, G.; MacDiarmid, A.G.; Epstein, A.J. *Synth. Met.* **1995,** *69*, 251.
77. Rånby, B.; Rabek, J.F. *ESR Spectroscopy in Polymer Research*, Springer-Verlag: Berlin, Heidelberg, New York, 1977.
78. Dubinski, A.A.; Grinberg, O.Y.; Kurochkin, V.I.; Oransky, L.G.; Poluektov, O.G.; Lebedev, Y.S. *Teor. Eksper. Khim.* **1981,** *17*, 231.
79. Hyde, J.S.; Dalton, L.R. In *Spin Labeling II: Theory and Application*, Berliner, L.J., Ed.; Academic Press: New York, 1979; Vol. 2, Chapt. 1, pp. 1–70.
80. Hustedt, E.J.; Beth, A.H. *Biophys. J.* **2004,** *86*, 3940.
81. Masubuchi, S.; Imai, R.; Yamazaki, K.; Kazama, S.; Takada, J.; Matsuyama, T. *Synth. Met.* **1999,** *101*, 594.
82. Wasserman, A.M.; Kovarski, A.L. *Spin Labels and Probes in Physics and Chemistry of Polymers (Russ)*, Nauka: Moscow, 1986.
83. *Spin Labeling: The Next Millenium*, Berliner, L.J., Ed.; Plenum Press: New York, 1998.
84. Pelekh, A.E.; Goldenberg, L.M.; Krinichnyi, V.I. *Synth. Met.* **1991,** *44*, 205.
85. Buchachenko, A.L. *Complexes of Radicals and Molecular Oxygen with Organic Molecules (Russ)*, Nauka: Moscow, 1984.
86. Reddoch, A.; Konishi, S. *J. Chem. Phys.* **1979,** *70*, 2121.
87. Kanemoto, K.; Yamauchi, J. *Phys. Rev. B* **2000,** *61*, 1075.
88. Krinichnyi, V.I.; Lebedev, Y.S.; Grinberg, O.Y. *Appl. Magn. Reson.* **1997,** *13*, 259.